THESIS FOR THE DEGREE OF DOCTOR OF PHILOSOPHY

Channel Prediction and Target Tracking for Multi-Agent Systems

Markus Fröhle

CHALMERS
UNIVERSITY OF TECHNOLOGY

Communication Systems Group
Department of Electrical Engineering
Chalmers University of Technology
Gothenburg, Sweden, 2018

Channel Prediction and Target Tracking for Multi-Agent Systems

Markus Fröhle
ISBN 978-91-7597-837-6

Doktorsavhandlingar vid Chalmers tekniska högskola
Ny serie Nr 4518
ISSN 0346-718X

This thesis has been prepared using LaTeX.

Communication Systems Group
Department of Electrical Engineering
Chalmers University of Technology
SE-412 96 Gothenburg, Sweden
Phone: +46 (0)31 772 1000
www.chalmers.se

Printed by Chalmers Digital Print
Gothenburg, Sweden, November 2018

Abstract

Mobile moving agents as part of a multi-agent system (MAS) utilize the wireless communication channel to disseminate information and to coordinate between each other. This channel is error-prone and the transmission quality depends on the environment as well as on the configuration of the transmitter and the receiver. For resource allocation and task planning of the agents, it is important to have accurate, yet computationally efficient, methods for learning and predicting the wireless channel. Furthermore, agents utilize on-board sensors to determine both their own state and the states of surrounding objects. To track the states over time, the objects' dynamical models are combined with the sensors' measurement models using a Bayesian filter. Through fusion of posterior information output by the agents' filters, the awareness of the agents is increased. This thesis studies the uncertainties involved in the communication and the positioning of MASs and proposes methods to properly handle them.

A framework to learn and predict the wireless channel is proposed, based on a Gaussian process model. It incorporates deterministic path loss and stochastic large scale fading, allowing the estimation of model parameters from measurements and an accurate prediction of the channel quality. Furthermore, the proposed framework considers the present location uncertainty of the transmitting and the receiving agent in both the learning and the prediction procedures. Simulations demonstrate the improved channel learning and prediction performance and show that by taking location uncertainty into account a better communication performance is achieved.

The agents' location uncertainties need to be considered when surrounding objects (targets) are estimated in the global frame of reference. Sensor impairments, such as an imperfect detector or unknown target identity, are incorporated in the Bayesian filtering framework. A Bayesian multitarget tracking filter to jointly estimate the agents' and the targets' states is proposed. It is a variant of the Poisson multi-Bernoulli filter and its performance is demonstrated in simulations and experiments. Results for MASs show that the agents' state uncertainties are reduced by joint agent-target state tracking compared to tracking only the agents' states, especially with high-resolution sensors.

While target tracking allows for a reduction of the agents' state uncertainties, high-resolution sensors require special care due to multiple detections per target. In this case, the tracking filter needs to explicitly model the dimensions of the target, leading to extended target tracking (ETT). An ETT filter is combined with a Gaussian process shape model, which results in accurate target state and shape estimates. Furthermore, a method to fuse posterior information from multiple ETT filters is proposed, by means of minimizing the Kullback-Leibler average. Simulation results show that the adopted ETT filter accurately tracks the targets' kinematic states and shapes, and posterior fusion provides a holistic view of the targets provided by multiple ETT filters.

Keywords: Multi-agent system, channel prediction, Gaussian processes, location uncertainty, multitarget tracking, extented target tracking, posterior fusion.

List of Publications

This thesis is based on the following publications:

(A) M. Fröhle, T. Charalambous, I. Nevat, and H. Wymeersch, "Channel Prediction with Location Uncertainty for Ad Hoc Networks," in *IEEE Transactions on Signal and Information Processing over Networks*, vol. 4, no. 2, pp. 349–361, June 2018.

(B) M. Fröhle, L. S. Muppirisetty, and H. Wymeersch, "Channel Gain Prediction for Multi-agent Networks in the Presence of Location Uncertainty," in *Proceedings of IEEE International Conference on Acoustics, Speech and Signal Processing (ICASSP)*, pp. 3911–3915, Shanghai, China, 2016.

(C) M. Fröhle, C. Lindberg, and H. Wymeersch, "Cooperative Localization of Vehicles without Inter-vehicle Measurements," in *Proceedings of IEEE Wireless Communications and Networking Conference (WCNC)*, pp. 1–6, Barcelona, Spain, 2018.

(D) M. Fröhle, C. Lindberg, K. Granström, and H. Wymeersch, "Multisensor Poisson Multi-Bernoulli Filtering for Joint Target-Sensor State Tracking," submitted to *IEEE Transactions on Intelligent Vehicles*, 2018.

(E) M. Fröhle, K. Granström, and H. Wymeersch, "Multiple Target Tracking with Uncertain Sensor State Applied to Autonomous Vehicle Data," in *Proceedings of IEEE Statistical Signal Processing Workshop (SSP)*, pp. 628–632, Freiburg, Germany, 2018.

(F) M. Fröhle, K. Granström, and H. Wymeersch, "Decentralized Poisson Multi-Bernoulli Filtering for Extended Target Tracking," submitted to *IEEE Transactions on Aerospace and Electronic Systems*, 2018.

Publications by the author not included in the thesis:

(a) M. Fröhle, A. A. Zaidi, E. Ström, and H. Wymeersch, "Multi-Step Sensor Selection with Position Uncertainty Constraints," in *Proceedings of 2014 IEEE Globecom Workshops*, pp. 1439–1444, Austin, TX, 2014.

(b) M. Fröhle, and H. Wymeersch, "On the Separation of Timescales in Radio-based Positioning," in *Proceedings of 2015 International Conference on Location and GNSS (ICL-GNSS)*, Gothenburg, Sweden, 2015.

(c) S. Zhang, M. Fröhle, H. Wymeersch, A. Dammann, and R. Raulefs, "Location-Aware Formation Control in Swarm Navigation," in *Proceedings of 2015 IEEE Globecom Workshops*, San Diego, CA, 2015.

(d) F. Meyer, H. Wymeersch, M. Fröhle, and F. Hlawatsch, "Distributed Estimation With Information-Seeking Control in Agent Networks," in *IEEE Journal on Selected Areas in Communications*, vol. 33, no. 11, pp. 2439–2456, Nov. 2015.

(e) M. Fröhle, "Channel Gain Prediction for Cooperative Multi-Agent Systems," *Licentiate Thesis*, Gothenburg, Sweden, Oct. 2016.

(f) O. Daniel, J. Raasakka, P. Peltola, M. Fröhle, A. Rivero-Rodriguez, H. Wymeersch, and J. Nurmi, "Blind sub-Nyquist GNSS signal detection," in *Proceedings of IEEE International Conference on Acoustics, Speech and Signal Processing (ICASSP)*, pp. 6575–6579, Shanghai, China, 2016.

(g) M. Fröhle, T. Charalambous, H. Wymeersch, S. Zhang, and A. Dammann, "Formation Control of Multi-Agent Systems with Location Uncertainty," in *Multi-Technology Positioning*, Springer, pp. 197–215, 2017.

(h) V. Chowdappa, M. Fröhle, H. Wymeersch, and C. Botella, "Distributed Channel Prediction for Multi-Agent Systems," in *Proceedings of IEEE International Conference on Communications (ICC)*, pp. 1–6, Paris, France, 2017.

(i) H. Wymeersch, N. Garcia, H. Kim, G. Seco-Granados, S. Kim, F. Wen, and M. Fröhle, "5G mmWave Downlink Vehicular Positioning," in *Proceedings of 2018 IEEE Globecom Workshops*, pp. 1–7, Abu Dhabi, United Arab Emirates, 2018.

Acknowledgments

Once upon a time, we set course up North, passed by a small town called Göteborg, where we put up our tent. The day after, I reported for duty on a close-by island called Chalmers. Prof. Henk Wymeersch, tasked with my supervision, turned out to be knowledgeable, keen on pursuing the research task, and had a sympathetic ear for my concerns (mostly through the semi-new communication media called electronic mail). Thankfully, he always had an advice/suggestion/path ahead I could follow. Thanks for your patience and commitment!

But wait, he was not alone. Prof. Erik Ström assisted and kept us all together at the Comsys group. Thanks! An on-island expedition resulted in the discovery of two great collaborators: Prof. Themis Charalambous and Dr. Karl Granström. I enjoyed working with you and bothering you with my many questions. Thanks!

Comsys: folks from different parts of the world (even Swedes) occupying a whole corridor, supporting and distracting me from my agreed task throughout these years: the thesis. I am very thankful for the contribution of every one of them including Agneta[1], Àlex, Andreas, Arni, Bile, Christopher, Cristian, Erik, Fredrik, Gabo, Giuseppe[1], Jie, Johan, Li, Mohammad, Nil, Rahul, Rebecka, Robert[1], Roman, Sven. Thanks!

From time to time, I was asked to leave the island to share and discuss with other fellows what I have learned. I met great people within MULTI-POS. Thanks for the great time we enjoyed in this project. I went to Honeywell and still don't know what the department where I resided works on. I spent a hot summer at DLR in a new, but uncooled building, with friendly and knowledgeable people who suffered the same fate. Thanks for the hospitality!

Experiments. Important, time consuming, but thanks to the great people at Revere a hard-/software issue was quickly resolved (or at least identified). Thanks for your assistance!

My family planted the faith in me that everything is possible. It was fed well by their endless support and trust. For that I am very happy and thankful. Danke!
The biggest thanks belong to you, Isabel. You had to sacrifice a lot so that I could follow my dream. I am very happy that you chose to join me on this expedition. You give me the strength, support, patience, and good mood to make grumpy me smile. Grazas, meu amor!

Markus Fröhle
Göteborg, November 2018

[1] Not Comsys, but in same department.

Financial support

This work is supported, in part, by the European Research Council under grant no. 258418 (COOPNET), by EU FP7 Marie Curie Initial Training Network MULTI-POS (Multi-technology Positioning Professionals) under grant no. 316528, by the EU H2020 project HIGHTS (High Precision Positioning for Cooperative ITS Applications) under grant no. MG-3.5a-2014-636537, and by the COPPLAR (campus shuttle cooperative perception and planning platform) project, funded under grant no. 2015-04849 from Vinnova.

Contents

Part I

Overview

CHAPTER 1

Introduction

1.1 Motivation

Mobile agents that communicate and perceive the environment through their on-board sensors form a multi-agent system (MAS). They disseminate information and coordinate with each other using the wireless channel. Typical examples of MAS include mobile wheel-driven robots for surveillance and search-and-rescue operations, or unmanned aerial vehicless (UAVs) for remote sensing, e.g., to detect forest fires [1] or for chemical plume tracking [2]. Examples within the context of intelligent transportation systems (ITSs) include autonomous cars cooperating on sensor data or for throughput maximization at an intersection [3], [4].

Since mobile agents employ the wireless medium for communication, it is important to have accurate, yet computationally efficient, methods to learn and predict the wireless channel allowing them to pursue their higher-level tasks successfully. This includes channel prediction, i.e., when knowledge of the channel is needed for configurations of the agents where no measurements are available. The wireless channel depends on the environment as well as the positions of transmitter (TX) and receiver (RX). Its properties have been well studied and accurate channel and propagation models have been developed, mainly for cellular communication systems [5]. Channel models for communication between mobile agents are less explored [6]–[10]. One reason for this was the lack of use cases. Such a channel model is more complex, since it needs to consider mobility of both link endpoints. Accurate channel prediction and parameter estimation requires the location of the mobile agents (equipped with TX/RX units) to be known exactly. In reality however, mobile agents estimate their location based on measure-

ments provided by sensors such as a Global Positioning System (GPS) receiver. Due to measurement errors, the true location of the agent is not known exactly. Uncertainty about the agent's location should therefore be incorporated into the channel learning and prediction process.

Furthermore, the agents utilize their on-board sensors to observe the environment. Examples include radars, lidars, or stereo vision cameras. The state (e.g., position and velocity) of mobile objects present in the environment can be tracked with the help of a tracking filter, which combines the object's dynamical model with the sensor's measurement model in a Bayesian framework. An example is the Kalman filter for Gaussian linear models [11].

With potentially multiple objects (targets) present, a multitarget tracking (MTT) filter can be employed to estimate the presence and the kinematic state of multiple (independently) moving objects from measurements [12], [13]. Typically, the estimated state of the objects is represented in the sensor's (relative) coordinate frame. When the object's state should be represented in the global (absolute) coordinate frame, e.g., for sharing of environment information within the MAS, the location uncertainty of the platform, where the sensor is mounted on, needs to be considered in the tracking filter.

Traditionally, MTT has been developed for sky surveillance using ground-to-air radars. The resolution of such a radar was low compared to the size of an airplane observed at a large distance. It was sufficient to assume that each measurement may be caused by one airplane. In contrast, with novel automotive radars and lidars, a single object can produce multiple measurements within one measurement scan (one measurement round). Using such high-resolution sensors, requires the incorporation of the shape of the tracked objects within the tracking filter. An extended target tracking (ETT) filter considers, additionally to an MTT filter, the extent of each object [14]. Several ETT filters have been proposed in literature, often as extensions of their MTT filter counterpart. Depending on the application, more or less detailed models can be used to describe and estimate the target's extent with a ETT filter.

Agents then utilize the wireless channel to disseminate target information within the MAS. Due to the limited bandwidth available of the communication channel, it is not attractive to directly share raw measurement data obtained by a high-resolution sensor. Instead, filtered information as output from a tracking filter can be shared, e.g., in the form of parameter values of a known distribution [15]. The agent then fuses the received target information with information provided by its own tracking filter. To not deteriorate estimation performance, any correlation among the target estimates need to be considered in the fusion process.

1.2 Challenges and Proposed Solutions

This thesis considers challenges involved in agent-to-agent communication and target tracking, relevant for mobile MAS. The addressed challenges and proposed solutions are

listed below.

- Both communication and positioning are affected by uncertainties. In Paper A and B, we propose a framework based on Gaussian processs (GPs) to model, learn, and predict the wireless channel between mobile agents (modeling deterministic path-loss and spatially correlated shadowing). It allows to naturally incorporate the agents' location uncertainty for estimation of the channel parameters and for channel prediction. We apply the proposed channel prediction framework to an agent placement problem, where we demonstrate, in simulations, that incorporating location uncertainties, through the proposed model, leads to a better average communication performance compared to neglecting them.

- In MTT, location uncertainty of the platform, where the sensor is mounted on, needs to be considered when the target state should be estimated in the global coordinate frame. In Paper C, we propose a factor graph (FG) based approach for joint sensor-target state tracking with known number of targets, but unknown measurement-to-target association. Simulation results show that with the proposed approach the unknown associations are resolved and target tracking with uncertain sensor locations is possible. Furthermore, we observe that in a multi-agent scenario, the agents benefit by a reduced location uncertainty when local sensor state information is combined with target tracking information, compared to only using local sensor state information.
  In Paper D and E, we propose a Poisson multi-Bernoulli filter for joint sensor-target state tracking. Thereby, local sensor state information is fused with multisensor MTT information. We demonstrate the improved target tracking performance, in simulations and with real vehicular sensor data, when the uncertain sensor state is accounted for. Furthermore, we observe like in the FG based approach of Paper C, that in a multi-agent scenario, the location uncertainty of agents can be reduced through target tracking compared to agent state tracking alone, especially with high-resolution sensors.

- In ETT, the sensor obtains potentially multiple detections per target, which requires modeling of the target shape. Furthermore, information collected by multiple filters need to be fused correctly to produce reliable estimates. In Paper F, we apply a Gaussian process model in a novel ETT filter (c.f. [16], [17]) to estimate and track the shape and kinematic state of multiple extended targets (ETs). Furthermore, we propose a method for robust fusion of posterior information, collected by multiple independent ETT filters, in the minimum Kullback-Leibler average (KLA) sense. Simulation results show the proposed filter accurately tracks the targets presence, kinematic state and shape. Furthermore, we observe that posterior fusion allows to provide a holistic view of the targets. The result is an improved tracking performance compared to the performance achieved by each individual ETT filter alone.

1.3 Thesis Outline

This thesis is divided into two parts. Part I provides an overview of the concepts used in the appended papers. In particular, Chapter 2 discusses the wireless propagation channel. Indoor channel measurements, which were used in Paper A, are presented. In Chapter 3, Gaussian process regression is discussed. It is utilized for channel prediction in Papers A and B, as well as in Paper F to describe the star-convex shape of extended targets. In Chapter 4, vector-based Bayesian target tracking is introduced. Different estimators and linear filters are discussed. Also addressed are incorporation of an uncertain sensor state and fusion of information. The discussion is extended in Chapter 5 to set-based MTT, where a small background on random finite sets (RFSs) is given, together with relevant RFS based MTT filters. Furthermore, ETT is briefly discussed in the chapter. Related to this chapter, Paper E presents a RFS based MTT filter, and Paper F presents a decentralized RFS based ETT filter. Chapter 6 summarizes the scientific achievements, presents the conclusions of this thesis and gives directions for future work. Part II of this thesis consists of the appended Papers A–F.

CHAPTER 2

The Wireless Propagation Propagation Channel

In this chapter, we present indoor channel measurements for the wireless propagation channel, where both the transmitter (TX) and the receiver (RX) are mobile. This is followed by the presentation of a known empirical statistical channel model, which we relate to the collected measurements and discuss briefly its validity. Following that, we highlight two spatial correlation models, one where only the RX is mobile, and one where both, the TX and the RX are mobile. This forms the basis for the channel prediction framework proposed in Papers A and B.

2.1 Overview

In general, the wireless channel can be considered as being composed of three parts: a part due to path-loss, a part due to shadowing because of obstacles, and a part due to multi-path [5]. Shadowing is spatially correlated and measurements have shown that it decorrelates in the order of 50–100 m outdoors [5] and 1–5 m indoors [18], [19]. Multi-path, on the other hand, decorrelates on a much smaller scale within a few wavelengths [5]. Based on this, several different channel models have been developed. The most simple model is the disc model, where communication quality is assumed *good* if the RX is located within a radius r of the TX and *bad* otherwise. The next step towards a more accurate model considers deterministic path-loss. More sophisticated channel models incorporate also shadowing and multi-path. These components are modeled either in a probabilistic or a deterministic way (e.g., through ray-tracing [5]). Although more accurate, such models come with some drawbacks. For instance, an accurate ray-tracing

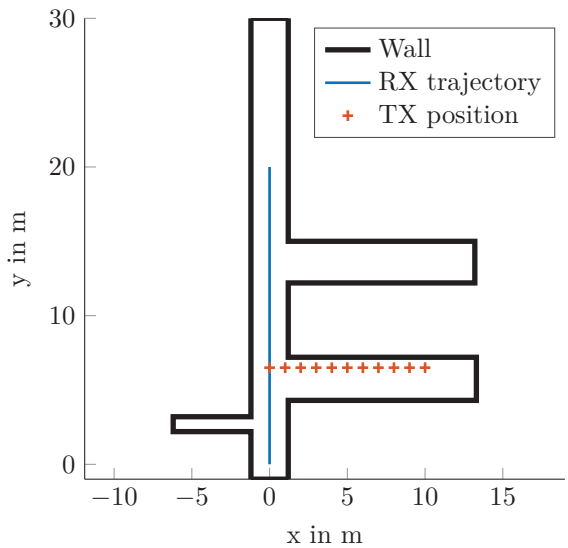

Figure 2.1. Floorplan together with TX and RX locations where channel measurements have been recorded. All walls consist of reinforced concrete. For every TX position, the RX moved along the indicated RX trajectory recording every 0.02 m the received signal power in dBm.

based channel model may not be applicable in real-time applications due to the high computational demand. Furthermore, it is not always possible to estimate all model parameters from measurements, e.g., for ray-tracing this means that reflection properties of all surfaces in the environment need to be estimated. This becomes infeasible in complex operating environments and one then needs to restrict to simplified environment models, which as a result, reduce the accuracy of ray-tracing.

2.2 Indoor Channel Measurements

In order to justify any model assumptions in the development of our channel prediction framework of Papers A and B, we have performed a measurement campaign, where we recorded indoor channel measurements in a hallway at the Department of Electrical Engineering at Chalmers University of Technology. For this campaign, we placed the RX at several different positions along a line following the hallway. On a hallway perpendicular to it, we placed the TX on several different positions also along a line, where the first location thereby corresponds to position 6.5 m on the RX line. The full measurement scenario is outlined in Fig. 2.1. For every position of the TX and RX, the received power in dBm was recorded using commodity hardware radios of type *Netgear N150 Wireless adapter*. The measurement parameters are stated in Table 1.

Table 2.1. Measurement parameters

Parameter	Value
Total number of different RX positions	10,900
Total number of different TX positions	11
Spatial resolution RX positions	0.02 m
Spatial resolution TX positions	1 m
Shortest TX-RX distance	1 m
Transmit power P_{TX}	20 dBm
Antenna height	0.85 m
Carrier frequency	2.422 GHz
Transmission bandwidth	20 MHz

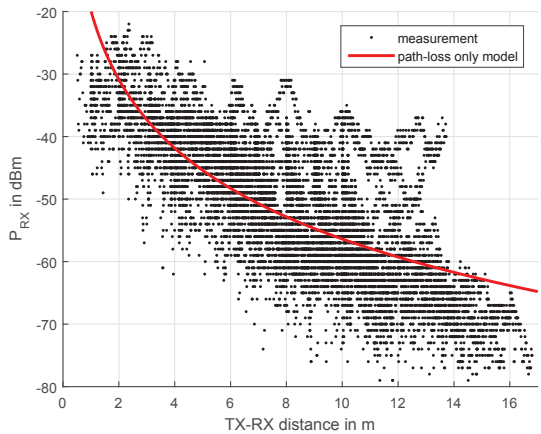

Figure 2.2. Measured received power in dBm with respect to TX-RX Euclidean distance. The received power following model (2.2) and ignoring any present spatial correlation is plot in red.

In Fig. 2.2, the received signal power in dBm is plotted over the distance between the TX and RX locations. Note that the hardware used provides the received power readings only in integer dBm values. From the figure, we can observe a power loss with increasing distance, but due to the complexity of the indoor propagation environment it is difficult to come up with an accurate and computationally efficient channel model. We are therefore interested in a simple channel model, which captures the signal propagation sufficiently well with respect to its application. It should be noted that any such model is only an approximation of the real channel.

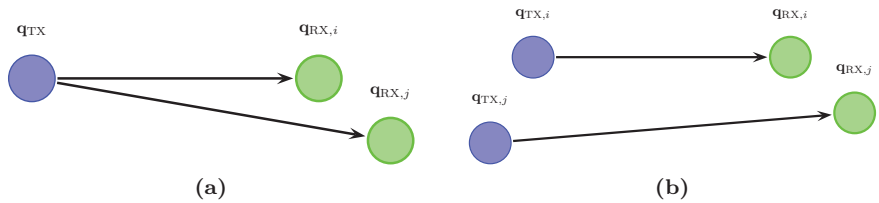

Figure 2.3. Left: The Gudmundson correlation model considers wireless communication links between different RX locations for a common TX location. Right: A correlation model suitable for mobile agent to mobile agent communication needs to consider wireless communication links where the TX locations differ as well.

2.3 Statistical Channel Model

Consider a workspace $\mathcal{W} \subset \mathbb{R}^2$. The TX located at $\boldsymbol{q}_{\mathrm{TX}} \in \mathcal{W}$ emits a signal with power $P_{\mathrm{TX}}^{\mathrm{lin}}$ through the wireless channel. Until the signal is received at the RX located at $\boldsymbol{q}_{\mathrm{RX}} \in \mathcal{W}$, it experiences distance-dependent path-loss, large-scale fading caused by obstacles in the propagation path, and small-scale fading due to multi-path. The received signal power can be expressed as [20]

$$P_{\mathrm{RX}}^{\mathrm{lin}}(\boldsymbol{q}_{\mathrm{TX}}, \boldsymbol{q}_{\mathrm{RX}}) = P_{\mathrm{TX}}^{\mathrm{lin}} g_0 \, ||\boldsymbol{q}_{\mathrm{TX}} - \boldsymbol{q}_{\mathrm{RX}}||_2^{-\eta} \psi(\boldsymbol{q}_{\mathrm{TX}}, \boldsymbol{q}_{\mathrm{RX}}) \, |h(\boldsymbol{q}_{\mathrm{TX}}, \boldsymbol{q}_{\mathrm{RX}})|^2, \tag{2.1}$$

where g_0 is a constant capturing antenna and other propagation gains, η is the path-loss exponent, ψ is the position dependent shadowing and h captures small-scale fading. Let us assume that measurements average out small-scale fading, either in time (measurements taken over a time window), frequency (measurements represent average power over a large frequency band), or space (by using multiple antennas) the received signal power in dBm is then expressed as

$$P_{\mathrm{RX}}(\boldsymbol{q}_{\mathrm{TX}}, \boldsymbol{q}_{\mathrm{RX}}) = L_0 - 10\eta \log_{10} ||\boldsymbol{q}_{\mathrm{TX}} - \boldsymbol{q}_{\mathrm{RX}}||_2 + \Psi(\boldsymbol{q}_{\mathrm{TX}}, \boldsymbol{q}_{\mathrm{RX}}), \tag{2.2}$$

where L_0 is the average received power in dBm at distance d_0, and $\Psi(\boldsymbol{q}_{\mathrm{TX}}, \boldsymbol{q}_{\mathrm{RX}}) = 10 \log_{10} \psi(\boldsymbol{q}_{\mathrm{TX}}, \boldsymbol{q}_{\mathrm{RX}})$. We assume that large-scale fading (shadowing) follows a log-normal distribution, i.e., $\Psi(\boldsymbol{q}_{\mathrm{TX}}, \boldsymbol{q}_{\mathrm{RX}}) \sim \mathcal{N}(0, \sigma_\Psi^2)$, where σ_Ψ^2 is the shadowing variance [5].

Remark: *For a static propagation environment and homogeneous TX and RX units, the transmission channel can be considered reciprocal [21]. This means if the roles of TX and RX units are interchanged, the instantaneous channel characteristics remain the same. In* (2.2)*, the part due to path-loss only depends on the distance between TX and RX and is therefore independent of the TX/RX roles. The second part of* (2.2) *models shadowing and to ensure channel reciprocity holds, we need to ensure that* $\Psi(\mathbf{q}_{TX}, \mathbf{q}_{RX}) = \Psi(\mathbf{q}_{RX}, \mathbf{q}_{TX})$ *(c.f. [5], [20]).*

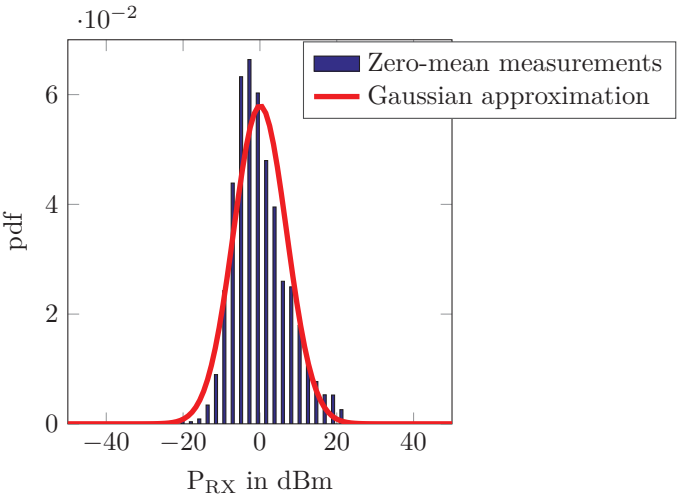

Figure 2.4. Empirical pdf of zero-mean measurements $\boldsymbol{y}_c$ plot in blue bars. A Gaussian approximation is plot in red.

Shadowing is, in general, spatially correlated, i.e., RX locations which are spatially close to each other experience similar shadow fading. For instance, if the TX-RX propagation path is blocked at one RX location, it may be also blocked at close-by RX locations with respect to the obstacle dimensions.

For a common TX endpoint $\mathbf{q}_{\mathrm{TX}} \in \mathcal{W}$, a well-known correlation model is the Gudmundson model for different RX locations $\mathbf{q}_{\mathrm{RX},i}, \mathbf{q}_{\mathrm{RX},j} \in \mathcal{W}$ [22]. This case is illustrated in Fig. 2.3a. The covariance between RX i and j with zero-mean measurements $\boldsymbol{y}_{c,i}$ and $\boldsymbol{y}_{c,j}$ follows an exponential decay, i.e.,

$$C_{ij}^{G}(d_{ij}) = \sigma_{\Psi}^{2} \exp\left(-\frac{d_{ij}}{d_c}\right), \tag{2.3}$$

where $d_{ij} = \|\boldsymbol{q}_{\mathrm{RX},i} - \boldsymbol{q}_{\mathrm{RX},j}\|$ and d_c is the decorrelation distance.

This model can be extended to account for communication links with non-common TX endpoints $\mathbf{q}_{\mathrm{TX},i}, \mathbf{q}_{\mathrm{TX},j} \in \mathcal{W}$ (see, for example [23], [24]), under the assumption that the TX–RX distance is large compared to the displacement between the TX endpoints and the RX endpoints. This case is illustrated in Fig. 2.3b. The covariance under this model becomes [23]

$$C_{ij}^{W}(d_{\mathrm{TX},ij}, d_{\mathrm{RX},ij}) = \sigma_{\Psi}^{2} \exp\left(-\frac{d_{\mathrm{TX},ij}}{d_c}\right) \exp\left(-\frac{d_{\mathrm{RX},ij}}{d_c}\right), \tag{2.4}$$

where $d_{\mathrm{TX},ij} = \|\boldsymbol{q}_{\mathrm{TX},i} - \boldsymbol{q}_{\mathrm{TX},j}\|$ and similarly for the RX. For brevity, we omit a discussion on the validity of these correlation models and instead refer the reader to [22]–[24]. Note,

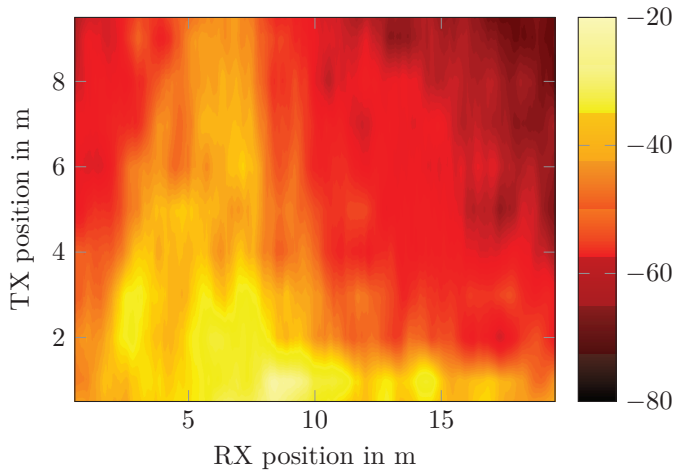

Figure 2.5. Recorded received power in dBm for different TX and RX positions. The TX moved perpendicular to the RX starting at RX position 6.5 m. Measurements have been spatially averaged to remove small-scale fading.

both presented models only depend on the distances between the link endpoints thus maintaining channel reciprocity.

2.4 Measurement-Model Relationship

We assume the RX provides us with a noisy observation of the received signal power in dBm such that

$$y = P_{\mathrm{RX}}(\boldsymbol{q}_{\mathrm{TX}}, \boldsymbol{q}_{\mathrm{RX}}) + n, \tag{2.5}$$

where $n \sim \mathcal{N}(0, \sigma_n^2)$ and σ_n^2 is the measurement noise variance. In order to make (2.2) applicable, we need to ensure multi-path is not present in y. For this, we have performed spatial averaging over a distance of 0.4 m along the RX trajectory, where the wavelength of the transmitted signal is approx. 0.12 m. Assuming now (2.2) holds, we can determine the channel constants L_0 and η via least-squares (LS) estimation. From our measurements, we have obtained $\hat{L}_0 = -19.88$ dBm and $\hat{\eta} = 3.65$. The model (2.2) is plot in red in Fig. 2.2 using the estimated parameters. In (2.2), shadowing Ψ is assumed Gaussian with variance σ_Ψ^2. To verify this is valid, we remove the mean from the measurements and plot in Fig. 2.4 the empirical pdf on the mean removed received power together with a Gaussian fit, where we found $\Psi \sim \mathcal{N}(0.04, 6.88^2)$.[1] From the figure, we observe that shadowing is not exactly Gaussian distributed. It has a positive skew but, with respect

[1] Note, the used hardware radios did not provide access to σ_n^2 as stated in (2.5). Therefore, the measurement noise variance is absorbed σ_Ψ^2.

to accuracy and complexity of the channel model, a Gaussian approximation may still be reasonable.

The spatial correlation of shadowing can be well observed in the recorded measurements. In Fig. 2.5, the received signal power in dBm is plot in color for different TX and RX positions. The RX position indicates the position along the RX trajectory (in vertical direction) as shown in Fig. 2.1, and similarly for the TX position (in horizontal direction). A line-of-sight (LOS) situation occurs when the RX is around position 6.5 m (corresponding to $x = 0$ m and $y = 6.5$ m in Fig. 2.1) resulting in high received signal power. For RX positions more distant than 6.5 m a non-LOS (NLOS) situation occurs due to the blockage from the wall.

2.5 Summary

We observed from indoor channel measurements that a deterministic path-loss model alone is not sufficient to explain the received signal power accurately. Furthermore, we saw that received signal power is spatially correlated depending on the environment and the positions of the TX and RX. These facts are utilized in Papers A and B, where we exploit the spatial correlation of shadowing additional to the deterministic path-loss for channel gain prediction. The Gaussian nature of shadowing as defined in (2.2) allows to utilize Gaussian processs (GPs), which are described in the next chapter.

CHAPTER 3

Gaussian Process Regression

In this chapter, we introduce Gaussian process (GP) regression, which has been used in Papers A, B and F. First, we define the GP model and address then the two important phases of GPs: (i) learning of the underlying model parameters, and (ii) prediction of a (non-linear) function at an unvisited location with the help of a measurement database. Second, we make use of the GP framework in the context of channel prediction addressing both, the learning phase to determine the underlying channel parameters from measurements, and the prediction phase allowing to predict the wireless channel between arbitrary transmitter and receiver locations. Finally, we show how GPs can be utilized to model star-convex object shapes.

3.1 Standard Gaussian Process

3.1.1 Model

According to [25], a GP is defined as a probability distribution over functions $f(\boldsymbol{x})$ such that the set of values $f(\boldsymbol{x})$ evaluated at an arbitrary set of points $\boldsymbol{x}_1, \boldsymbol{x}_2, \ldots, \boldsymbol{x}_N$ jointly have a Gaussian distribution.

We write the GP of a real stochastic process $f(\boldsymbol{x}) \in \mathbb{R}$ with input $\boldsymbol{x} \in \mathbb{R}^D$ as [26]

$$f(\boldsymbol{x}) \sim \mathcal{GP}(\mu(\boldsymbol{x}), k(\boldsymbol{x}, \boldsymbol{x}')) \tag{3.1}$$

with mean function

$$\mu(\boldsymbol{x}) = \mathbb{E}[f(\boldsymbol{x})] \tag{3.2}$$

and covariance function (also called kernel function)

$$k(\boldsymbol{x}, \boldsymbol{x}') = \mathbb{E}[(f(\boldsymbol{x}) - \mu(\boldsymbol{x})(f(\boldsymbol{x}') - \mu(\boldsymbol{x}')]. \tag{3.3}$$

Many choices of kernel functions are available of which the γ-exponential family is commonly selected. It is given by [26]

$$k(\boldsymbol{x}, \boldsymbol{x}') = \exp\left(-\left(\frac{\|\boldsymbol{x} - \boldsymbol{x}'\|}{l}\right)^{\gamma}\right), \tag{3.4}$$

where l denotes the characteristic length-scale and $0 < \gamma \leq 2$. The exponential kernel is obtained for $\gamma = 1$ and the squared exponential kernel for $\gamma = 2$. A necessary and sufficient condition for a kernel to be valid is that the resulting Gram matrix $\boldsymbol{K}$ with entries $\boldsymbol{K}_{ij} = k(\boldsymbol{x}_i, \boldsymbol{x}_j)$, $\forall \boldsymbol{x}_i, \boldsymbol{x}_j$ is positive semidefinite [25]. A way of constructing valid new kernels is to combine valid (simpler) kernels following some rules. As an example, consider two valid kernels $k_1(\boldsymbol{x}, \boldsymbol{x}')$ and $k_2(\boldsymbol{x}, \boldsymbol{x}')$. Then valid kernels are constructed by [25]

$$k_3(\boldsymbol{x}, \boldsymbol{x}') = ck_1(\boldsymbol{x}, \boldsymbol{x}'), \tag{3.5}$$

$$k_4(\boldsymbol{x}, \boldsymbol{x}') = k_1(\boldsymbol{x}, \boldsymbol{x}') + k_2(\boldsymbol{x}, \boldsymbol{x}'), \tag{3.6}$$

$$k_5(\boldsymbol{x}, \boldsymbol{x}') = k_1(\boldsymbol{x}_a, \boldsymbol{x}'_a)k_2(\boldsymbol{x}_b, \boldsymbol{x}'_b), \tag{3.7}$$

where $c > 0$ is a positive constant and $\boldsymbol{x} = [\boldsymbol{x}_a^{\mathsf{T}}, \boldsymbol{x}_b^{\mathsf{T}}]^{\mathsf{T}}$ (not necessarily disjoint). There exist more rules to construct valid kernels, but rules (3.5), (3.6), and (3.7) will turn out to be sufficient for our studies.

In order to incorporate measurements of the function $f(\boldsymbol{x})$ in the GP model, e.g., for regression, we need to consider any present measurement noise. The measurement model is given by

$$y = f(\boldsymbol{x}) + n, \tag{3.8}$$

where we assume $n \sim \mathcal{N}(0, \sigma_n^2)$. The GP model parameters are collected in a vector $\boldsymbol{\theta}$ and comprise the parameters of the mean function $\mu(\boldsymbol{x})$, the kernel function $k(\boldsymbol{x}, \boldsymbol{x}')$, as well as the measurement noise standard deviation σ_n.

The joint distribution of measurements $\boldsymbol{y} = [y_1, y_2, \ldots, y_N]^{\mathsf{T}}$ with inputs $\boldsymbol{X} = [\boldsymbol{x}_1, \boldsymbol{x}_2, \ldots, \boldsymbol{x}_N]$ is Gaussian with

$$p(\boldsymbol{y}|\boldsymbol{X}, \boldsymbol{\theta}) = \mathcal{N}(\boldsymbol{\mu}(\boldsymbol{X}), \boldsymbol{C}), \tag{3.9}$$

where $\boldsymbol{\mu}(\boldsymbol{X}) = [\mu(\boldsymbol{x}_1), \mu(\boldsymbol{x}_2), \ldots, \mu(\boldsymbol{x}_N)]^{\mathsf{T}}$ and $\boldsymbol{C}_{ij} = \boldsymbol{K}_{ij} + 1_{\{i=j\}}\sigma_n^2$. Here, $1_{\{I=J\}} = 1$ for $I = J$ and 0 otherwise. The measurement database comprising all N measurements is denoted by $\mathcal{D} = \{\boldsymbol{X}, \boldsymbol{y}\}$. With $\mathcal{D}$, the GP model parameters $\boldsymbol{\theta}$ can be learned. Once the learning phase is complete, the function value $f(\boldsymbol{x}_*)$ for an arbitrary input $\boldsymbol{x}_*$ can be predicted. Learning and prediction phases are explained next.

3.1.2 Learning Phase

Here, we are interested in estimating $\boldsymbol{\theta}$ from $\mathcal{D}$. The maximum likelihood (ML) estimator for $\boldsymbol{\theta}$ is obtained by minimizing the negative log-likelihood with respect to $\boldsymbol{\theta}$. It can be written as

$$\hat{\boldsymbol{\theta}} = \arg\min_{\boldsymbol{\theta}} \{-\log p(\boldsymbol{y}|\boldsymbol{X}, \boldsymbol{\theta})\} \tag{3.10}$$

$$= \arg\min_{\boldsymbol{\theta}} \left\{\log |\boldsymbol{C}| + (\boldsymbol{y} - \boldsymbol{\mu}(\boldsymbol{X}))^{\mathsf{T}} \boldsymbol{C}^{-1} (\boldsymbol{y} - \boldsymbol{\mu}(\boldsymbol{X}))\right\}, \tag{3.11}$$

where $\boldsymbol{C}$ and $\boldsymbol{\mu}$ depend on $\boldsymbol{\theta}$. Note that the negative log-likelihood is in general non convex.

Although a global search is optimal, it comes with the drawback of a high computational cost. A computationally more attractive approach is to perform a local search via a gradient based method. In [27], it is pointed out that such an approach often leads to a local minimum which might not explain the data well. This can be minimized by performing an maximum a posteriori (MAP) estimation over the hyperparameters instead of ML estimation. In doing so, the hyperparameter vector is treated as a random vector (RV) with known prior probability density function (PDF) $p(\boldsymbol{\theta})$. The MAP estimator is

$$\hat{\boldsymbol{\theta}}^{\mathrm{MAP}} = \arg\max_{\boldsymbol{\theta}} p(\boldsymbol{\theta}|\boldsymbol{y}, \boldsymbol{X}) = \arg\max_{\boldsymbol{\theta}} p(\boldsymbol{y}|\boldsymbol{X}, \boldsymbol{\theta}) p(\boldsymbol{\theta}). \tag{3.12}$$

In this way, the prior on the hyperparameters will act as a regularization term such that unlikely hyperparameters will not lead to a local minimum. Since we assume there is no prior knowledge on $\boldsymbol{\theta}$ available, we cannot follow this approach here.

3.1.3 Prediction Phase

With the GP model parameters $\boldsymbol{\theta}$ and the training database $\mathcal{D}$ at hand, we are ready to determine the predictive distribution of $f(\boldsymbol{x}_*)$ for the arbitrary input $\boldsymbol{x}_*$. It is given by [26]

$$p(f(\boldsymbol{x}_*)|\mathcal{D}, \boldsymbol{\theta}) = \mathcal{N}(m(\boldsymbol{x}_*), \sigma^2(\boldsymbol{x}_*)) \tag{3.13}$$

with mean

$$m(\boldsymbol{x}_*) = \mu(\boldsymbol{x}_*) + \boldsymbol{k}_*^{\mathsf{T}} \boldsymbol{C}^{-1} (\boldsymbol{y} - \boldsymbol{\mu}(\boldsymbol{X})) \tag{3.14}$$

and variance

$$\sigma^2(\boldsymbol{x}_*) = k_{**} - \boldsymbol{k}_* \boldsymbol{C}^{-1} \boldsymbol{k}_*^{\mathsf{T}}, \tag{3.15}$$

where $k_{**} = k(\boldsymbol{x}_*, \boldsymbol{x}_*)$ and $\boldsymbol{k}_* = [k(\boldsymbol{x}_1, \boldsymbol{x}_*), k(\boldsymbol{x}_2, \boldsymbol{x}_*), \ldots, k(\boldsymbol{x}_N, \boldsymbol{x}_*)]^{\mathsf{T}}$.

3.2 Gaussian Process with Uncertain Inputs

So far, we have considered the input $\boldsymbol{x}$ of a GP to be known and hence deterministic. In practice, this is seldom the case. Consider for instance that $\boldsymbol{x}$ represents the position of an agent. This quantity needs to be estimated from (noisy) measurements and therefore, we need to model it as a random variable. Then, the earlier presented GP framework, which considers $\boldsymbol{x}$ to be deterministic, cannot be applied anymore.

To see this, consider $\boldsymbol{x}_* \sim \mathcal{N}(\boldsymbol{u}_*, \Sigma_{\boldsymbol{x}_*})$. The predictive distribution $f(\boldsymbol{u}_*)$ is obtained by [28]

$$p(f(\boldsymbol{u}_*)|\mathcal{D}, \boldsymbol{u}_*, \Sigma_{\boldsymbol{x}_*}, \boldsymbol{\theta}) = \int p(f(\boldsymbol{x}_*)|\mathcal{D}, \boldsymbol{x}_*, \boldsymbol{\theta}) p(\boldsymbol{x}_*|\boldsymbol{u}_*, \Sigma_{\boldsymbol{x}_*}) \mathrm{d}\boldsymbol{x}_*, \tag{3.16}$$

which is not Gaussian anymore since

$$p(f(\boldsymbol{x}_*)|\mathcal{D}, \boldsymbol{x}_*, \boldsymbol{\theta}) = \frac{1}{\sqrt{2\pi\sigma^2(\boldsymbol{x}_*)}} \exp\left(-\frac{(f(\boldsymbol{x}_*) - m(\boldsymbol{x}_*))^2}{2\sigma^2(\boldsymbol{x}_*)}\right), \tag{3.17}$$

which is nonlinear in $\boldsymbol{x}_*$. According to [27], [28], we can approximate the predictive distribution by a Gaussian PDF

$$p(f(\boldsymbol{u}_*)|\mathcal{D}, \boldsymbol{u}_*, \Sigma_{\boldsymbol{x}_*}, \boldsymbol{\theta}) \approx \mathcal{N}(m(\boldsymbol{u}_*, \Sigma_{\boldsymbol{x}_*}), \sigma^2(\boldsymbol{u}_*, \Sigma_{\boldsymbol{x}_*})), \tag{3.18}$$

where $m(\boldsymbol{u}_*, \Sigma_{\boldsymbol{x}_*})$ and $\sigma^2(\boldsymbol{u}_*, \Sigma_{\boldsymbol{x}_*})$ are obtained by computing the mean and variance of (3.16), i.e.,

$$m(\boldsymbol{u}_*, \Sigma_{\boldsymbol{x}_*}) = \int a \; p(a|\mathcal{D}, \boldsymbol{u}_*, \Sigma_{\boldsymbol{x}_*}, \boldsymbol{\theta}) \mathrm{d}a, \tag{3.19}$$

$$\sigma^2(\boldsymbol{u}_*, \Sigma_{\boldsymbol{x}_*}) = \int a^2 \; p(a|\mathcal{D}, \boldsymbol{u}_*, \Sigma_{\boldsymbol{x}_*}, \boldsymbol{\theta}) \mathrm{d}a - m(\boldsymbol{u}_*, \Sigma_{\boldsymbol{x}_*})^2. \tag{3.20}$$

Note, for the special case of the squared exponential kernel, where $\gamma = 2$ in (3.4) and the PDF of $\boldsymbol{x}_*$ is Gaussian, closed form expressions for the expected moments exist. Furthermore, uncertainty in the input $\boldsymbol{x}_*$ not only occurs in the prediction phase as we have highlighted here. Also uncertainty in the training set $\boldsymbol{X}$ might be present, which affects both learning of the model parameters and prediction. For ease of discussion, we omit the implications of uncertainty in the training set. However, we address this in detail in the appended Papers A and B.

3.3 GP Regression for Channel Gain Prediction

Here, we are interested in modeling the received signal power (in dBm) as a GP with inputs $\boldsymbol{x} = [\boldsymbol{q}_{\mathrm{TX}}^{\mathsf{T}}, \boldsymbol{q}_{\mathrm{RX}}^{\mathsf{T}}]^{\mathsf{T}}$ consisting of the transmitter (TX) location $\boldsymbol{q}_{\mathrm{TX}} \in \mathcal{W}$ and the

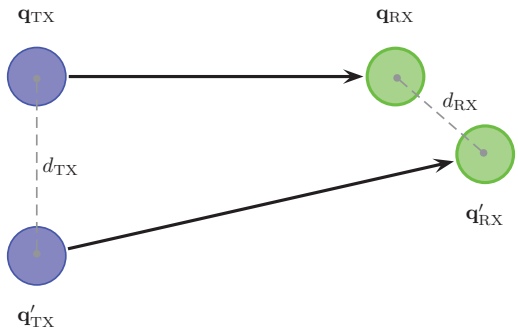

Figure 3.1. Illustration of TX distance d_{TX} and RX distance d_{RX} between two links $\boldsymbol{x}$ and $\boldsymbol{x}'$.

receiver (RX) location $\boldsymbol{q}_{\mathrm{TX}} \in \mathcal{W}$, respectively. Then

$$P_{\mathrm{RX}}(\mathbf{x}) \sim \mathcal{GP}(\mu_{\mathrm{cGP}}(\mathbf{x}), c_{\mathrm{cGP}}(\mathbf{x}, \mathbf{x}')). \tag{3.21}$$

The mean $\mu_{\mathrm{cGP}}(\mathbf{x})$ is obtained by computing the expectation of (2.2) with respect to the large-scale fading $\Psi(\mathbf{x})$, yielding

$$\mu_{\mathrm{cGP}}(\mathbf{x}) = L_0 - 10\eta \log_{10} ||\mathbf{q}_{\mathrm{TX}} - \mathbf{q}_{\mathrm{RX}}||_2. \tag{3.22}$$

Under the assumption that spatial channel correlation is isotropic, it can be characterized by the Euclidean distance d_{TX} between the TX locations of two communication links $\boldsymbol{x}$ and $\boldsymbol{x}'$, and by their RX distance d_{RX}, respectively. This relationship is illustrated in Fig. 3.1. Therefore, we adapt the covariance function of [29] to incorporate the TX state by

$$k(\mathbf{x}, \mathbf{x}') = \sigma_\Psi^2 \exp\left(-\frac{d_{\mathrm{TX}}^\gamma}{d_c^\gamma}\right) \exp\left(-\frac{d_{\mathrm{RX}}^\gamma}{d_c^\gamma}\right), \tag{3.23}$$

where $d_{\mathrm{TX}} = \|\mathbf{q}_{\mathrm{TX}} - \mathbf{q}'_{\mathrm{TX}}\|$, $d_{\mathrm{RX}} = \|\mathbf{q}_{\mathrm{RX}} - \mathbf{q}'_{\mathrm{RX}}\|$, parameter σ_Ψ^2 denotes the variance of the shadowing process. The parameter d_c is the decorrelation distance. For $\gamma = 1$ we have the model of [23], and if one of the link endpoints distance is zero, which is the case if $\boldsymbol{q}_{\mathrm{TX}} = \boldsymbol{q}'_{\mathrm{TX}}$ or $\boldsymbol{q}_{\mathrm{RX}} = \boldsymbol{q}'_{\mathrm{RX}}$, we obtain the Gudmundson model [22]. Assuming the noise power σ_n^2 is known, the hyper-parameter vector is $\boldsymbol{\theta} = [L_0, \eta, \sigma_\Psi, d_c]^\mathsf{T}$.

Remark: *The GP framework as introduced previously does not consider channel reciprocity per se. The reason for this is that, through the definition of the input vector* $\boldsymbol{x} = [\boldsymbol{q}_{\mathrm{TX}}^\mathsf{T}, \boldsymbol{q}_{\mathrm{RX}}^\mathsf{T}]^\mathsf{T}$*, an implicit ordering has been introduced. There are several ways how channel reciprocity can be ensured: by applying an operator on the input vector* $\boldsymbol{x}$ *to make it independent from the* link direction*, by modifying the kernel function, or by extending the measurement database by its reciprocal counterpart. In our work, we have chosen the latter approach, where for every measurement* y_i *recored at TX-RX location pair* $\boldsymbol{x}_i$ *an*

additional entry in the database $\mathcal{D}$ is made with the same measurement, but where the role of TX and RX are interchanged in $\boldsymbol{x}_i$.

3.4 GP Regression for Modeling Star-Convex Shapes

A GP can also be used to model the shape of a star convex object. A set $\mathcal{S}$ is star-convex if all possible line segments from the center to any point in $\mathcal{S}$ are in the set. We follow the approach proposed by [30]. Assuming the object is centered at the origin, the GP is defined

$$f(\phi) \sim \mathcal{GP}(\mu(\phi), k(\phi, \phi)), \tag{3.24}$$

where ϕ is the input angle and $f(\phi)$ the object boundary. Assuming an a priori object shape of a circle, the mean function is defined $\mu(\phi) = r$, where r is the known object radius. The proposed covariance function is defined as [30]

$$k(\phi, \phi') = \sigma_f^2 \exp\left(-\frac{2\sin^2\left(\frac{|\phi-\phi'|}{2}\right)}{l^2} \right), \tag{3.25}$$

where σ_f, and l are the (known) model hyper-parameters. Note that this function is 2π periodic, i.e., $k(\phi + 2\pi, \phi') = k(\phi, \phi')$. When the radius r is unknown, we can adjust the GP model (3.24). Let

$$r \sim \mathcal{N}(r_0, \sigma_r^2) \tag{3.26}$$

with mean r_0 and variance σ_r^2. Then (3.24) can be rewritten as

$$f(\phi) \sim \mathcal{GP}(r_0, \tilde{k}(\phi, \phi')), \tag{3.27}$$

$$\tilde{k}(\phi, \phi') = k(\phi, \phi') + \sigma_r^2. \tag{3.28}$$

In Fig. 3.2 the covariance function $\tilde{k}(\phi, 0)$ is plotted for different values of ϕ. From the figure, we observe that the covariance is highest for $\phi = \phi'$ and decreases as $|\phi - \phi'|$ increases from 0 to π. The hyperparameter vector of this GP model is $\boldsymbol{\theta} = [l, \sigma_f, \sigma_r]^\mathsf{T}$. We utilize this GP model in Paper F to describe the shape of objects tracked by an extended target tracking (ETT) filter.

3.5 Summary

GPs are an attractive tool for modeling stochastic processes. Measurements of the process are incorporated in the form of a database, and by conditioning on it, the predictive distribution of the process for an arbitrary input value is obtained in closed form.

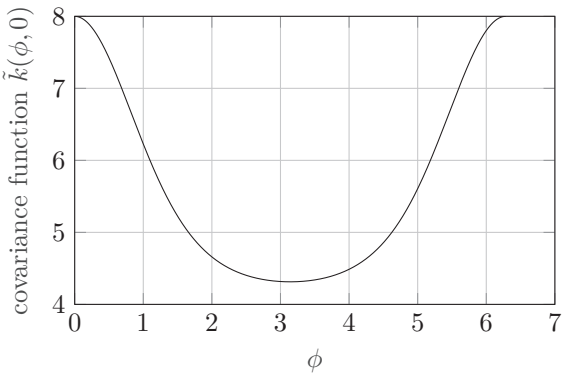

Figure 3.2. The covariance function $\tilde{k}(\phi, 0)$ is plot for hyperparameters $\sigma_f = 2$, $\sigma_r = 2$, and $l = \sqrt{\pi}/2$.

Furthermore, the underlying hyperparameter of the GP model can be learned from measurements. We saw that a GP can be used to model deterministic path-loss and spatial correlation of large scale fading of the wireless communication channel between mobile agents. This is used in Papers A and B, where we adapt the GP to incorporate any present location uncertainty of the TX and RX. Furthermore, we saw that a GP can be used to describe the (unknown) shape of a star-convex object. In Paper F, we utilize a GP to model the shape of extended targets (ETs) inside an ETT filter.

CHAPTER 4

Bayesian Target Tracking

In this chapter, we introduce the reader to the concept of Bayesian state estimation. Different estimators as well as an exact solution for the state estimation problem, in the form of the Kalman filter (KF), and an approximate filter, in the form of the extended Kalman filter (EKF), are presented. We also discuss how uncertainty of the sensor state, e.g., an uncertain location of the platform on which the sensor is mounted, can be incorporated in the state estimation problem. Furthermore, we discuss two different approaches for Bayesian state estimation to handle a multi-sensor setup depending on the available computation and communication resources.

4.1 Optimal Bayesian Estimation

In target tracking, we are interested in estimating the time-varying state of a target (i.e., the object of interest) from measurements. Let the target state at discrete time $k \in \mathbb{N}$ be described by the random vector (RV) $\boldsymbol{x}_k \in \mathbb{R}^{n_x}$.[1] Its evolution over time can be described by [31]

$$\boldsymbol{x}_k = f_{k-1}(\boldsymbol{x}_{k-1}, \boldsymbol{v}_{k-1}), \tag{4.1}$$

where f_{k-1} is a known possibly non-linear function and $\boldsymbol{v}_{k-1}$ is independent identically distributed (IID) process noise. Furthermore, the state $\boldsymbol{x}_k$ is observed by a sensor pro-

[1] For brevity, we limit the discussion here to discrete-time systems. See, e.g., [11] for a discussion on state estimation in continuous-time systems.

viding measurement $\boldsymbol{z}_k \in \mathbb{R}^{n_z}$ with measurement model

$$\boldsymbol{z}_k = h_k(\boldsymbol{x}_k, \boldsymbol{n}_k), \tag{4.2}$$

where h_k is a known possibly non-linear function and $\boldsymbol{n}_k$ is IID measurement noise. We are interested in the state $\boldsymbol{x}_k$ in every discrete time step k from all measurements $\boldsymbol{z}_{1:k} = [\boldsymbol{z}_1^\mathsf{T}, \ldots, \boldsymbol{z}_k^\mathsf{T}]^\mathsf{T}$ up to time k. This Bayesian estimation problem is illustrated Fig. 4.1. With a known prior belief of the state $\boldsymbol{x}$ at time $k = 0$ in the form of the probability density function (PDF) $p(\boldsymbol{x}_0)$, we can cast the tracking problem recursively in a Bayesian framework. Hence, we seek to calculate the posterior PDF $p(\boldsymbol{x}_k|\boldsymbol{z}_{1:k})$ in every time step k, which can be calculated by alternating a prediction and an update step, i.e., we seek a filtered estimate of $\boldsymbol{x}_k$ from measurements $\boldsymbol{z}_{1:k}$. The prediction step utilizes the process model (4.1) via the Chapman-Kolmogorov equation to obtain the prior PDF at time step k. It is given by

$$p(\boldsymbol{x}_k|\boldsymbol{z}_{1:k-1}) = \int p(\boldsymbol{x}_k, \boldsymbol{x}_{k-1}|\boldsymbol{z}_{1:k-1}) \mathrm{d}\boldsymbol{x}_{k-1} \tag{4.3}$$

$$= \int p(\boldsymbol{x}_k|\boldsymbol{x}_{k-1}, \boldsymbol{z}_{1:k-1}) p(\boldsymbol{x}_{k-1}|\boldsymbol{z}_{1:k-1}) \mathrm{d}\boldsymbol{x}_{k-1} \tag{4.4}$$

$$= \int p(\boldsymbol{x}_k|\boldsymbol{x}_{k-1}) p(\boldsymbol{x}_{k-1}|\boldsymbol{z}_{1:k-1}) \mathrm{d}\boldsymbol{x}_{k-1}, \tag{4.5}$$

where the last equality comes from the fact that (4.1) describes a first-order Markov model. With the measurement $\boldsymbol{z}_k$, provided by the sensor, the predicted prior PDF is updated via the Bayes rule. The obtained posterior PDF is

$$p(\boldsymbol{x}_k|\boldsymbol{z}_{1:k}) = \frac{p(\boldsymbol{z}_k|\boldsymbol{x}_k) p(\boldsymbol{x}_k|\boldsymbol{z}_{1:k-1})}{p(\boldsymbol{z}_k|\boldsymbol{z}_{1:k-1})} \tag{4.6}$$

with

$$p(\boldsymbol{z}_k|\boldsymbol{z}_{1:k-1}) = \int p(\boldsymbol{z}_k|\boldsymbol{x}_k) p(\boldsymbol{x}_k|\boldsymbol{z}_{1:k-1}) \mathrm{d}\boldsymbol{x}_k. \tag{4.7}$$

Here, the measurement likelihood function $p(\boldsymbol{z}_k|\boldsymbol{x}_k)$ is described by the measurement model (4.2) and the known statistics of $\boldsymbol{n}_k$. Note that this implies $p(\boldsymbol{z}_k|\boldsymbol{x}_k, \boldsymbol{z}_{1:k-1}) = p(\boldsymbol{z}_k|\boldsymbol{x}_k)$. The prediction and update step form the basis of recursively calculating the Bayesian optimal solution for which, in general, no analytical solution exist.

4.2 Bayesian Estimators

Here, we review different estimation approaches for $\boldsymbol{x}_k$. The source of this is [32].

The minimum mean square error (MMSE) estimator assumes that the joint PDF

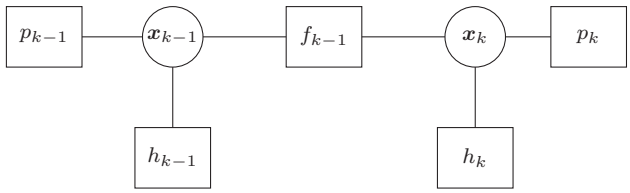

Figure 4.1. Illustration of the Bayesian estimation problem. The prior PDF is given by $p_{k-1}(\boldsymbol{x}_{k-1}) \triangleq p(\boldsymbol{x}_{k_1}|\boldsymbol{z}_{1:k-1})$ and the posterior PDF is given by $p_k(\boldsymbol{x}_k) \triangleq p(\boldsymbol{x}_k|\boldsymbol{z}_{1:k})$, respectively.

$p(\boldsymbol{x}_k, \boldsymbol{z}_{1:k})$ is known. The estimator is defined with respect to (w.r.t.) the posterior $p(\boldsymbol{x}_k|\boldsymbol{z}_{1:k})$ as

$$\hat{\boldsymbol{x}}_k^{\mathrm{MMSE}} = \int \boldsymbol{x}_k p(\boldsymbol{x}_k|\boldsymbol{z}_{1:k}) \mathrm{d}\boldsymbol{x}_k. \tag{4.8}$$

For general PDFs, this estimator is difficult to implement and approximate methods need be used, e.g., particle filters [31], [33]. The KF can be seen as a particular implementation of the linear MMSE (LMMSE) estimator defined recursively (c.f. [11]), thus providing a closed form solution of (4.1) and (4.2) for Gaussian linear state evolution and measurement models.

The maximum a posteriori (MAP) estimator has the same model assumption as the MMSE estimator. The MAP estimator is defined as

$$\hat{\boldsymbol{x}}_k^{\mathrm{MAP}} = \arg\max_{\boldsymbol{x}_k} p(\boldsymbol{x}_k|\boldsymbol{z}_{1:k}) = \arg\max_{\boldsymbol{x}_k} p(\boldsymbol{z}_{1:k}|\boldsymbol{x}_k) p(\boldsymbol{x}_k). \tag{4.9}$$

The MAP and MMSE estimators are identical for PDFs where the mean and mode is the same.

4.3 LMMSE Filters

Here, we review the KF and EKF, both yielding the best linear estimate in the MMSE sense either exact or approximately. The source of this is [11]. Other LMMSE filters not reviewed here include the cubature Kalman filter (CKF) [34], and the unscented Kalman filter (UKF) [35], [36].

4.3.1 Kalman Filter

The KF assumes a linear Gaussian model for the process model (4.1) and measurement model (4.2). The state evolution is described by

$$\boldsymbol{x}_k = F_{k-1}\boldsymbol{x}_{k-1} + \boldsymbol{v}_{k-1}, \tag{4.10}$$

where F_{k-1} is a known matrix and $\boldsymbol{v}_{k-1}$ is white, zero-mean, uncorrelated noise with covariance matrix V_{k-1}. The state $\boldsymbol{x}_k$ is observed by

$$\boldsymbol{z}_k = H_k \boldsymbol{x}_k + \boldsymbol{n}_k, \tag{4.11}$$

where H_k is a known matrix, and $\boldsymbol{n}_k$ is white, zero-mean, uncorrelated noise with covariance matrix N_k. Additionally, $\boldsymbol{v}_{k-1}$ and $\boldsymbol{n}_k$ are uncorrelated, i.e., $\mathbb{E}[\boldsymbol{v}_{k-1}\boldsymbol{n}_k^\mathsf{T}] = \mathbf{0}$. With this model, the KF provides the Bayesian optimal solution to (4.5) and (4.6). The filter consists of alternating prediction and update steps. It is initialized as [11]

$$\hat{\boldsymbol{x}}_0 = \mathbb{E}[\boldsymbol{x}_0], \tag{4.12}$$
$$P_0^+ = \mathbb{E}[(\boldsymbol{x}_0 - \hat{\boldsymbol{x}}_0)(\boldsymbol{x}_0 - \hat{\boldsymbol{x}}_0)^\mathsf{T}]. \tag{4.13}$$

The prediction step is given by

$$P_k^- = F_{k-1} P_{k-1}^+ F_{k-1}^\mathsf{T} + V_{k-1}, \tag{4.14}$$
$$\hat{\boldsymbol{x}}_k^- = F_{k-1} \hat{\boldsymbol{x}}_{k-1}^+ \tag{4.15}$$

calculating the a priori state estimate $\hat{\boldsymbol{x}}_k^-$ with covariance P_k^-. The update step corrects the state estimate with measurement $\boldsymbol{z}_k$. It is given by

$$K_k = P_k^- H_k^\mathsf{T} (H_k P_k^- H_k^\mathsf{T} + N_k)^{-1}, \tag{4.16}$$
$$\hat{\boldsymbol{x}}_k^+ = \hat{\boldsymbol{x}}_k^- + K_k(\boldsymbol{z}_k - H_k \hat{\boldsymbol{x}}_k^-), \tag{4.17}$$
$$P_k^+ = (I - K_k H_k) P_k^-, \tag{4.18}$$

where I is the identity matrix of proper dimension. The update step calculates the a posteriori state estimate $\hat{\boldsymbol{x}}_k^+$ with covariance P_k^+.

4.3.2 Extended Kalman Filter

The EKF allows to incorporate non-linear process and measurement models through approximation. The models are linearized via first-order Taylor series expansion around the prior and the predicted prior. The process and measurement model are of form (4.1) and (4.2). The process noise $\boldsymbol{v}_{k-1}$ is zero mean with covariance matrix V_{k-1} and similarly the measurement $\boldsymbol{n}_k$ is zero mean with covariance matrix N_k. The filter initialization is the same as in the KF. The prediction step first linearizes the process model through a first-order Taylor series expansion around $\boldsymbol{x}_{k-1} = \hat{\boldsymbol{x}}_{k-1}^+$ and $\boldsymbol{v}_{k-1} = 0$, and then applies

the KF prediction step. It is described as follows [11]

$$F_{k-1} = \left.\frac{\partial f_{k-1}}{\partial \boldsymbol{x}}\right|_{\hat{\boldsymbol{x}}_{k-1}^{+}}, \tag{4.19}$$

$$L_{k-1} = \left.\frac{\partial f_{k-1}}{\partial \boldsymbol{v}}\right|_{\hat{\boldsymbol{x}}_{k-1}^{+}}, \tag{4.20}$$

$$P_k^{-} = F_{k-1} P_{k-1}^{+} F_{k-1}^{\mathsf{T}} + L_{k-1} V_{k-1} L_{k-1}^{\mathsf{T}}, \tag{4.21}$$

$$\hat{\boldsymbol{x}}_k^{-} = f_{k-1}(\hat{\boldsymbol{x}}_{k-1}^{+}, 0), \tag{4.22}$$

where F_{k-1} and L_{k-1} are the Jacobians w.r.t. the state and the process noise, respectively. The update step first linearizes the measurement model around $\boldsymbol{x}_k = \hat{\boldsymbol{x}}_k^{-}$ and $\boldsymbol{n}_k = 0$, and then applies the KF update step. It is described as follows [11]

$$H_k = \left.\frac{\partial h_k}{\partial \boldsymbol{x}}\right|_{\hat{\boldsymbol{x}}_k^{-}}, \tag{4.23}$$

$$M_k = \left.\frac{\partial h_k}{\partial \boldsymbol{n}}\right|_{\hat{\boldsymbol{x}}_k^{-}}, \tag{4.24}$$

$$K_k = P_k^{-} H_k^{\mathsf{T}} (H_k P_k^{-} H_k^{\mathsf{T}} + M_k N_k M_k^{\mathsf{T}})^{-1}, \tag{4.25}$$

$$\hat{\boldsymbol{x}}_k^{+} = \hat{\boldsymbol{x}}_k^{-} + K_k(\boldsymbol{z}_k - h_k(\hat{\boldsymbol{x}}_k^{-}, 0)), \tag{4.26}$$

$$P_k^{+} = (I - K_k H_k) P_k^{-}. \tag{4.27}$$

It should be pointed out that the EKF is only suitable for mildly non-linear system models due to the first-order Taylor approximation.

4.4 Uncertain Sensor State

Usually, it is assumed that the sensor state (e.g., position and orientation) is known when performing target tracking. However in reality, the sensor deployment can introduce an unknown bias, e.g., due to mounting tolerances. Furthermore, when the sensor is mounted on a moving platform, e.g., a vehicle, the position of the platform may not be known precisely. This can be problematic when the target state is represented in global frame of reference and not in the sensor frame of reference. When the sensor state uncertainty is non-negligible, it can be modeled in a stochastic manner, e.g., by treating it as an additional nuisance parameter when the sensor state itself is not of interest [37, Ch. 16], [38], or the (target) state vector $\boldsymbol{x}_k$ is augmented by the unknown sensor state leading to joint target-sensor state tracking [39], [40].

For the latter case, we are interested in the posterior $p(\boldsymbol{x}_{T,1:k}, \boldsymbol{x}_{S,1:k} | \boldsymbol{z}_{1:k})$, where $\boldsymbol{x}_{T,1:k}$ denotes the target state and $\boldsymbol{x}_{S,1:k}$ the sensor state up to time k. In the following, we highlight two approaches for joint target-sensor state tracking.

4.4.1 Rao-Blackwellization Approach

Using the general product rule for probability, we can decompose the posterior PDF into

$$p(\boldsymbol{x}_{T,1:k}, \boldsymbol{x}_{S,1:k}|\boldsymbol{z}_{1:k}) = p(\boldsymbol{x}_{T,1:k}|\boldsymbol{x}_{S,1:k}, \boldsymbol{z}_{1:k})p(\boldsymbol{x}_{S,1:k}|\boldsymbol{z}_{1:k}), \tag{4.28}$$

which can be computed efficiently using a Rao-Blackwellized particle filter, where the sensor state is represented by a set of weighted samples and the target state is estimated conditioned on the sensor state [41]–[43].

The multitarget case with M number of known targets can be handled by augmenting the state vector to $\boldsymbol{x}_{T,1:k} = [\boldsymbol{x}_{T,1:k,1}^{\mathsf{T}}, \ldots, \boldsymbol{x}_{T,1:k,M}^{\mathsf{T}}]^{\mathsf{T}}$. Since the conditioning of the targets is on the whole sensor trajectory, and under the assumption that the targets move independently, the targets in (4.28) become independent leading to [40]

$$p(\boldsymbol{x}_{T,1:k}|\boldsymbol{x}_{S,1:k}, \boldsymbol{z}_{1:k}) = \prod_{m=1}^{M} p(\boldsymbol{x}_{T,1:k,m}|\boldsymbol{x}_{S,1:k}, \boldsymbol{z}_{1:k}). \tag{4.29}$$

For the special case of stationary targets (denoted landmarks), i.e., $\boldsymbol{x}_{T,k,m} = \boldsymbol{x}_{T,m}$ for all k and all m, we obtain the simultaneous localization and mapping (SLAM) problem [40], [44]. The fact that landmarks are independent when conditioned on the whole sensor trajectory is utilized in the well-established FastSLAM algorithm where the sensor trajectory is tracked with the help of a particle filter and for each particle an independent EKF is used to estimate the landmarks [40].

4.4.2 Message-Passing Approach

Utilizing the mobility model (4.1), the measurement model (4.2), and under the assumption that targets move independently, we can rewrite (4.28) for M targets as

$$\begin{aligned} p(\boldsymbol{x}_{T,1:k}, \boldsymbol{x}_{S,1:k}|\boldsymbol{z}_{1:k}) \propto\ & p(\boldsymbol{x}_{S,0}) \prod_{m=1}^{M} p(\boldsymbol{x}_{T,0,m}) \prod_{t=1}^{k} p(\boldsymbol{x}_{S,t}|\boldsymbol{x}_{S,t-1}) \\ & \times \prod_{m=1}^{M} p(\boldsymbol{x}_{T,t,m}|\boldsymbol{x}_{T,t-1,m}) p(\boldsymbol{z}_{t,m}|\boldsymbol{x}_{S,t}, \boldsymbol{x}_{T,t,m}), \end{aligned} \tag{4.30}$$

where $\boldsymbol{z}_{t,m}$ denotes the measurement of the m-th target at time t and $\boldsymbol{z}_k = [\boldsymbol{z}_{k,1}^{\mathsf{T}}, \ldots, \boldsymbol{z}_{k,M}^{\mathsf{T}}]^{\mathsf{T}}$. The MMSE estimator for the m-th target at time k is (c.f. (4.8))

$$\hat{\boldsymbol{x}}_{T,k,m}^{\mathrm{MMSE}} = \int \boldsymbol{x}_{T,k,m} p(\boldsymbol{x}_{T,k,m}|\boldsymbol{z}_{1:k}) \mathrm{d}\boldsymbol{x}_{T,k,m}, \tag{4.31}$$

and similarly for the sensor state $\boldsymbol{x}_{S,k}$. The equation above involves the marginal PDF $p(\boldsymbol{x}_{T,k,m}|\boldsymbol{z}_{1:k})$, which can be obtained by marginalizing the joint PDF (4.28). Note

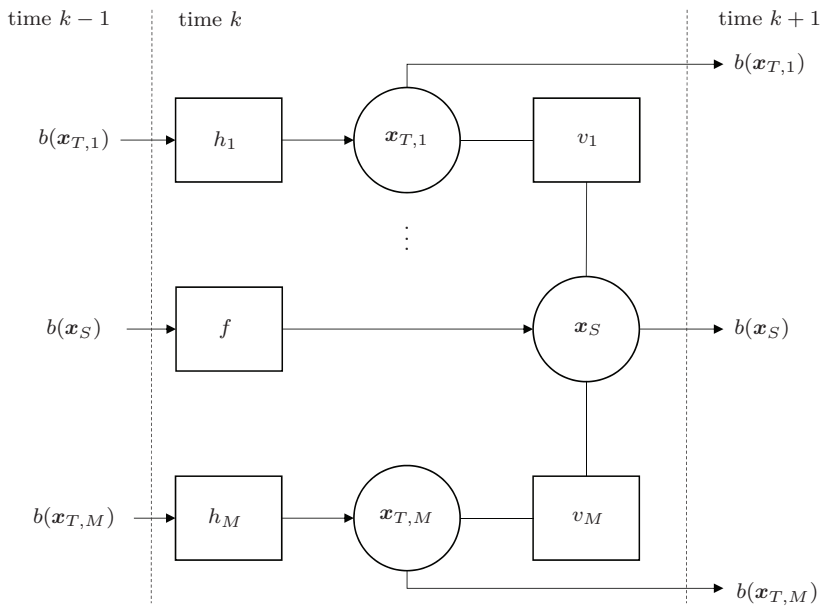

Figure 4.2. FG representation with M targets and a single sensor with uncertain state. Here, $h_m = p(\boldsymbol{x}_{T,k,m}|\boldsymbol{x}_{T,k-1,m})$, $f = p(\boldsymbol{x}_{S,k}|\boldsymbol{x}_{S,k-1})$, and $v_m = p(\boldsymbol{z}_{k,m}|\boldsymbol{x}_{S,k}, \boldsymbol{x}_{T,k,m})$. The time index has been omitted for brevity.

that the dimension of the joint PDF increases with time and direct calculation becomes infeasible. This problem can be obviated by direct calculation of the marginal PDFs with the help of message passing on the factor graph (FG) resulting of the factorization (4.30).[2]

The FG resulting (4.30) is illustrated in Fig. 4.2 for one time step. In the figure, variable nodes are drawn as circles and factor nodes, which take the RVs as arguments indicated by edges, are drawn as rectangles. The input at time k is the belief $b(\cdot)$, an approximation of the marginal PDF of the RV at time $k-1$ with associated edge. The beliefs at time k are then computed through message passing on the FG.

4.5 Data association

Until now, we assumed that it is known which measurement index in $\boldsymbol{z}_k$ belongs to which target at a particular time step. When this information is not present, a data association (DA) step needs to be performed. According to [37], there can be two different approaches for DA identified: non-Bayesian DA and Bayesian DA. In non-Bayesian DA, a decision is made based on a heuristic criterion, e.g., Euclidean distance, or based on

[2]See, e.g., [25, Ch. 8] or [45, Ch. 4] for an introduction on FGs.

a statistic tool like maximum likelihood (ML) or hypothesis testing. In Bayesian DA, probabilities of associations are computed and utilized throughout the estimation process.

An example for the non-Bayesian DA is to associate the target with maximum likelihood value among all measurements. Based on this hard decision, the measurement source is assumed known and can be used in the measurement update (4.6). Hence, DA is handled outside the Bayesian filtering framework. The DA step is executed in every time step prior to the measurement update.

An example for the Bayesian DA is probabilistic DA (PDA), which calculates the association probabilities for each measurement and the target, and if used in a tracking filter the PDA filter [12], [37]. In this filter, the prior target state is represented by a Gaussian PDF. After updating by M measurements, the posterior becomes a Gaussian mixture distribution with weights representing the DA. The algorithm then approximates the Gaussian mixture distribution by a single Gaussian in order to limit computational complexity.

The joint probability data association (JPDA) algorithm marginalizes over the joint DA to obtain the marginal DA for each target. This can be efficiently computed using loopy belief propagation (BP) on the corresponding FG [46]. We proceed with illustrating this method.

Let there be M targets with state $\boldsymbol{x}_{T,k,m}$ for $m = 1, \ldots, M$ at time k. For brevity, we further assume a perfect detection and no false alarm measurements, i.e., at each time step a measurement is generated from each target collected in vector $\boldsymbol{z}_k = [\boldsymbol{z}_{t,1}^{\mathsf{T}}, \ldots, \boldsymbol{z}_{t,M}^{\mathsf{T}}]^{\mathsf{T}}$ whose origin is unknown w.r.t. to the targets. Let variable $a_{k,n} = m \in \{1, \ldots, M\}$ indicate which measurement m at time k is hypothesized to target n, and let variable $b_{k,m} = n \in \{1, \ldots, M\}$ indicate which target n at time k is hypothesized to measurement m. Note that $a_{k,n}$ can be seen as a target oriented formulation of the DA and $b_{k,m}$ as a measurement oriented formulation, respectively. This formulation gives a one-to-one mapping between $a_{k,n}$ and $b_{k,m}$, i.e., if $a_{k,n}$ is known so is $b_{k,m}$. Let $\boldsymbol{a}_k = [a_{k,1}, \ldots, a_{k,M}]^{\mathsf{T}}$, and similarly for $\boldsymbol{b}_k$.

To ensure global consistency, in the sense that each measurement is associated to one and not more targets, we introduce the function [46]

$$\psi(a_{k,n}, b_{k,m}) = \begin{cases} 0, & a_{k,n} = m, b_{k,m} \neq n \text{ or } a_{k,n} \neq m, b_{k,m} = n, \\ 1, & \text{otherwise.} \end{cases} \tag{4.32}$$

We are now ready to update the joint posterior PDF of (4.30) to include the DA

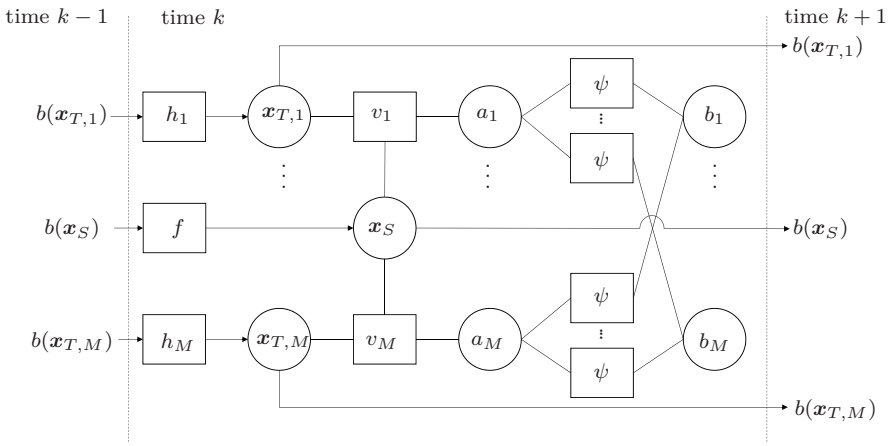

Figure 4.3. FG representation with M targets and measurements following the DA approach of [47]. Here, $h_m = p(\boldsymbol{x}_{T,t,m}|\boldsymbol{x}_{T,t-1,m})$ and $v_m = p(\boldsymbol{z}_{t,a_{k,m}}|\boldsymbol{x}_{S,t}, \boldsymbol{x}_{T,t,m})$. The time index has been omitted for brevity.

variables by

$$\begin{aligned} p(\boldsymbol{x}_{T,1:k}, \boldsymbol{x}_{S,1:k}, \boldsymbol{a}_{1:k}, \boldsymbol{b}_{1:k}|\boldsymbol{z}_{1:k}) \propto p(\boldsymbol{x}_{S,0}) \prod_{m=1}^{M} p(\boldsymbol{x}_{T,0,m}) \prod_{t=1}^{k} p(\boldsymbol{x}_{S,t}|\boldsymbol{x}_{S,t-1}) \\ \times \prod_{m=1}^{M} p(\boldsymbol{x}_{T,t,m}|\boldsymbol{x}_{T,t-1,m}) \\ \times \prod_{m'=1}^{M} p(\boldsymbol{z}_{t,a_{k,m}}|\boldsymbol{x}_{S,t}, \boldsymbol{x}_{T,t,m}) \psi(a_{k,m}, b_{k,m'}), \end{aligned} \tag{4.33}$$

where the measurement with index $a_{k,m}$ is used in the measurement likelihood. Similar to the message-passing approach of Sec. 4.4.2, the MMSE estimates of the sensor/target states require the knowledge of the marginal PDFs, computed by running loopy BP on the FG resulting of (4.33). The FG for a single time step is illustrated in Fig. 4.3. The FG part responsible for the DA (with variables $a_{k,m}$ and $b_{k,m}$) contains cycles and we solve this using loopy BP which iterates messages through the FG. After a fixed number of iterations or upon convergence, the outgoing message from $a_{k,m}$ to $v_{k,m}$ is found, which contains the approximate DA information considering the global consistency constraints. With the DA information, the updated beliefs of the sensor/target states can then be computed.

In Paper C, we consider a multisensor scenario with a factorization similar to (4.33). More details on the message passing solution can be found there. A limitation of this work is that the number of targets need to be a priori known. Related to this, [48]

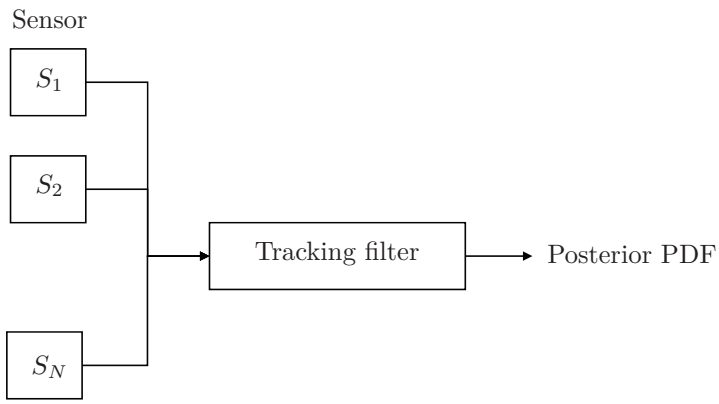

Figure 4.4. Illustration of likelihood fusion. At every time step k, each sensor S_s with $s = 1, \ldots, N$ obtains a measurement $\boldsymbol{z}_{s,k}$ and forwards it to the tracking filter, which outputs the posterior PDF $p(\boldsymbol{x}_k|\boldsymbol{z}_{1,1:k}, \ldots, \boldsymbol{z}_{N,1:k})$.

performs target tracking for an unknown number of targets, though the sensor state was assumed known.

4.6 Information Fusion

In a multisensor measurement scenario, measurements from all sensors are utilized for the calculation of the posterior PDF defined in (4.6). We can distinguish two setups:

- multiple sensors provide measurements to a single tracking filter, and where
- each sensor is equipped with a single tracking filter.

The former, called likelihood fusion, is illustrated in Fig. 4.4 and the later, called posterior fusion, is illustrated in Fig. 4.5.

4.6.1 Likelihood Fusion

With only one tracking filter, measurements from all sensors have to be incorporated in the measurement update step of the filter. Let $\boldsymbol{z}_{s,k}$ be the measurement from sensor s for $s = 1, \ldots, N$ received in time step k. We are therefore interested in the posterior PDF conditioned on measurements from all sensors, i.e., $p(\boldsymbol{x}_k|\boldsymbol{z}_{1,1:k}, \ldots, \boldsymbol{z}_{N,1:k})$. With only one tracking filter, and therefore only one prediction step, the measurement likelihood in (4.6) becomes

$$p(\boldsymbol{z}_k|\boldsymbol{x}_k) = p(\boldsymbol{z}_{1,k}, \ldots, \boldsymbol{z}_{N,k}|\boldsymbol{x}_k). \tag{4.34}$$

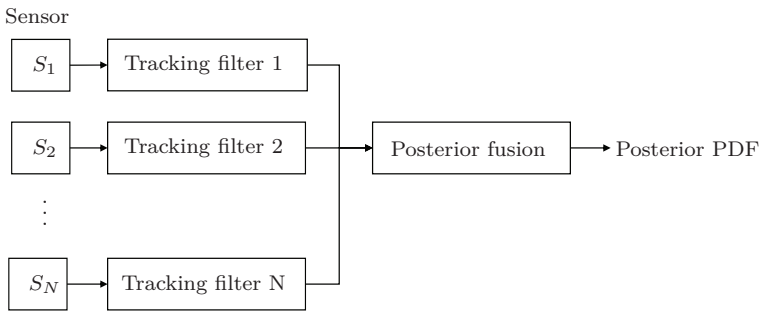

Figure 4.5. Illustration of posterior fusion. At every time step k, each sensor S_s with $s = 1, \ldots, N$ obtains a measurement $\boldsymbol{z}_{s,k}$ and forwards it to its tracking filter, which computes the posterior PDF $p(\boldsymbol{x}_k|\boldsymbol{z}_{s,1:k})$. This is then send to the posterior fusion block, which computes the posterior PDF $p(\boldsymbol{x}_k|\boldsymbol{z}_{1,1:k}, \ldots, \boldsymbol{z}_{N,1:k})$.

When the measurement noise conditioned on the system state is uncorrelated over all sensors, we can write

$$p(\boldsymbol{z}_k|\boldsymbol{x}_k) = \prod_{s=1}^{N} p(\boldsymbol{z}_{s,k}|\boldsymbol{x}_k), \tag{4.35}$$

where we have used the chain rule for conditional probability and the independence assumption due to the uncorrelated measurement noise. For instance, with linear Gaussian models and uncorrelated measurement noise over all sensors, (4.6) can then be solved using a KF by performing independent measurement update steps, one for each sensor.

4.6.2 Posterior Fusion

Target state estimates produced by different filters can be correlated. This can be caused by correlated estimation errors (measurement errors, common process noise, common prior) [49]. Any correlation among the target tracks, i.e., the information about a certain target, needs to be considered in the track fusion. For instance, with Gaussian posterior PDFs information decorrelation can be applied, where the common information is identified and removed in the fusion step [49]. The drawback of this procedure is that it requires to store the previous PDF and is only optimal then there is no process noise present.

When correlation is unknown, a suboptimal fusion of posterior information can be performed. In [50], [51], a robust fusion method for two Gaussian posterior PDFs called covariance intersection (CI) was presented. Note that robustness refers to the case that the uncertainty of the fused estimate in terms of the covariance matrix is conservative, i.e., it never underestimates the true uncertainty, but is also not too large [50], [52].

Assume two filter track the same target $\boldsymbol{x}$, where the posterior PDF at time step k can be described by the Gaussian PDF

$$p_i(\boldsymbol{x}_k|\boldsymbol{z}_{i,1:k}) = \mathcal{N}(\boldsymbol{x}_k; \hat{\boldsymbol{x}}_{i,k}, \hat{P}_{i,k}) \tag{4.36}$$

with mean vector $\hat{\boldsymbol{x}}_{i,k}$ and covariance matrix $\hat{P}_{i,k}$ for filters $i = \{1, 2\}$. The CI rule approximates the fused posterior PDF in terms of a Gaussian PDF with mean vector $\bar{\boldsymbol{x}}_k$ and covariance matrix $\bar{P}_k$ defined by [51]

$$\bar{P}_k^{-1} = \omega \hat{P}_{1,k}^{-1} + (1-\omega)\hat{P}_{2,k}^{-1}, \tag{4.37}$$

and

$$\bar{P}_k^{-1}\bar{\boldsymbol{x}}_k = \omega \hat{P}_{1,k}^{-1}\hat{\boldsymbol{x}}_{1,k} + (1-\omega)\hat{P}_{2,k}^{-1}\hat{\boldsymbol{x}}_{2,k}, \tag{4.38}$$

where $\omega \in [0, 1]$ is a weighting parameter. As pointed out by [52], the approximate fused estimate is unbiased and does not overstate the uncertainty of the fused estimate.

The CI fusion method can also be generalized to non-Gaussian posteriors leading to the constructed fused PDF [52]

$$p_\omega(\boldsymbol{x}_k|\boldsymbol{z}_{1,1:k}, \boldsymbol{z}_{2,1:k}) = \frac{p_1(\boldsymbol{x}_k|\boldsymbol{z}_{1,1:k})^\omega p_2(\boldsymbol{x}_k|\boldsymbol{z}_{2,1:k})^{1-\omega}}{\int p_1(\boldsymbol{x}_k|\boldsymbol{z}_{1,1:k})^\omega p_2(\boldsymbol{x}_k|\boldsymbol{z}_{2,1:k})^{1-\omega} \mathrm{d}\boldsymbol{x}_k}. \tag{4.39}$$

4.7 Summary

Bayesian filters allow to predict and update the state of a dynamic target through incorporation of measurements. We observed that exact filtering is possible, depending on the model assumptions. When these assumptions are violated, we need to restrict to approximate filtering. Furthermore, Bayesian filters allow to incorporate an uncertain sensor state. We identified two different setups of information fusion. With likelihood fusion there is a single filter, where the measurement likelihood of (4.6) incorporates measurements from all sensors. With posterior fusion, multiple independent tracking filters are present and any correlation between the target state estimates produced by the filters needs to be considered. Furthermore, with unknown correlation, suboptimal methods such as CI can be used. In the next chapter, we extend the discussion to Bayesian tracking with sets allowing to incorporate sensor properties such as an unknown target-to-measurement correspondence.

CHAPTER 5

Set-based Multitarget Tracking

In this chapter, we extend the discussion on Bayesian target tracking to set-based approaches. With the help of random finite sets, sensor properties, such as an imperfect detection, can be dealt with inside the Bayesian framework. Since optimal Bayesian estimation is intractable in general, approximate filters need to be used; we discuss multi-Bernoulli filters in more detail. We also extend our discussion on incorporation of sensor state uncertainty to set-based approaches. Furthermore, when the physical target size is big with respect to (w.r.t.) the sensor resolution, the point target assumption of multitarget tracking (MTT) filters does not hold anymore and this needs to be handled in the filter. We present common measurement and shape models for such extended targets (ETs). Finally, we extend our discussion on information fusion with multi-object posteriors.

5.1 Overview

An historic important application of MTT, i.e., tracking of independently moving targets, was, and is, the surveillance of the sky using ground-to-air radar sensors. Such a sensor has several peculiarities: it produces false alarm measurements due to clutter[1]; missed detections; unknown measurement-to-target correspondence; and target appearance and disappearance due to the limited sensor field-of-view (FoV). Such a sensor prohibits the application of Chapter 4 without further modifications.

[1] Note that clutter refers to any undesirable measurements not related to the state of interest, i.e., persistent clutter could be due to spurious energy reflectors, e.g., ground reflections, and random clutter could be due to objects or phenomena not related to the state of interest [12].

A MTT filter, on the other hand, incorporates the sensor peculiarities to perform the tracking task within the Bayesian framework. Thereby, one can distinguish between vector-type and set-type MTT filters. Probabilistic data association (DA) based methods for single target tracking treat the DA parameter as a nuisance parameter [53]. The probabilistic DA (PDA) filter represents the posterior probability density function (PDF) by a single Gaussian to keep computation complexity limited [54], where the joint probability data association (JPDA) filter extends this to multiple targets. Under the assumption that one target generates at most one measurement per sensor and time step, the joint DA is approximated by the product of marginal DAs for target [53]. Furthermore, factor graph (FG) based approaches, and extensions to unknown number of targets (joint integrated PDA (JIPDA) filter) exist [53], [55], [56]. A limitation of PDA based filters arises for spatially close targets, where the filter cannot distinguish between the individual targets anymore, which is a phenomenon called coalescence.

Set based methods model the target states and measurements by random finite sets (RFSs). An MTT filter based on RFSs allows to model the sensors' peculiarities inside the Bayesian filtering framework [57]. Let $\boldsymbol{X}_k$ be a RFS describing the target states at time step $k-1$ and let $\boldsymbol{Z}_k$ be a set containing the measurements received at time step k. The MTT filter can then be described, conceptually at least, within the Bayesian filtering framework by performing a prediction step using the motion model [57, Ch. 14]

$$f(\boldsymbol{X}_k|\boldsymbol{Z}_{1:k-1}) = \int f(\boldsymbol{X}_k|\boldsymbol{X}_{k-1}) f(\boldsymbol{X}_{k-1}|\boldsymbol{Z}_{1:k-1}) \delta \boldsymbol{X}_{k-1} \tag{5.1}$$

and a Bayesian update step

$$f(\boldsymbol{X}_k|\boldsymbol{Z}_{1:k}) = \frac{f(\boldsymbol{Z}_k|\boldsymbol{X}_k) f(\boldsymbol{X}_k|\boldsymbol{Z}_{1:k-1})}{\int f(\boldsymbol{Z}_k|\boldsymbol{X}_k) f(\boldsymbol{X}_k|\boldsymbol{Z}_{1:k-1}) \delta \boldsymbol{X}_k}, \tag{5.2}$$

where $f(\boldsymbol{X}_{k-1}|\boldsymbol{Z}_{1:k-1})$ is the prior RFS density, $f(\boldsymbol{X}_k|\boldsymbol{X}_{k-1})$ is the RFS transition density, $f(\boldsymbol{X}_k|\boldsymbol{Z}_{1:k-1})$ is the predicted RFS density, and $f(\boldsymbol{Z}_k|\boldsymbol{X}_k)$ is the RFS measurement likelihood for measurement set $\boldsymbol{Z}_k$. Note that the integrals above are set integrals (c.f. Section 5.2). In general, the calculation of the full multitarget posterior is intractable and approximations need to be applied.

5.2 Background on Random Finite Sets

In this section, we give some background information on RFSs.

An RFS $\boldsymbol{X}$ is a finite-set valued random variable, which can be described by a discrete probability distribution modeling the number of elements in $\boldsymbol{X}$ denoted by $p(n)$ with

$n \geq 0$, and a family of joint probability densities $f_n(\boldsymbol{x}_1, \ldots, \boldsymbol{x}_n)$ yielding [58]

$$f(\{\boldsymbol{x}_1, \ldots, \boldsymbol{x}_n\}) = p(n) \sum_{\sigma} f_n(\boldsymbol{x}_{\sigma(1)}, \ldots, \boldsymbol{x}_{\sigma(n)}), \tag{5.3}$$

where σ denotes a permutation of $\{1, \ldots, n\}$ and $\sigma(i)$ is the permutation of the i-th element. The sum spans all $n!$ possible permutations, such that its RFS density $f(\boldsymbol{X})$ becomes permutation invariant. The set integral of a real-valued function $g(\boldsymbol{X})$ of a finite-set variable $\boldsymbol{X}$ is defined as [57, p. 361]

$$\int g(\boldsymbol{X}) \delta \boldsymbol{X} \triangleq g(\emptyset) + \sum_{n=1}^{\infty} \frac{1}{n!} \int g(\{\boldsymbol{x}_1, \ldots, \boldsymbol{x}_n\}) \mathrm{d}\boldsymbol{x}_1 \cdots \mathrm{d}\boldsymbol{x}_n. \tag{5.4}$$

The probability hypothesis density (PHD), or intensity function, is the first order moment of the multitarget density formally defined as [59, eqn. (4.74)]

$$D(\boldsymbol{x}) = \int f(\{\boldsymbol{x}\} \cup \boldsymbol{W}) \delta \boldsymbol{W}, \tag{5.5}$$

where $f(\cdot)$ is an RFS density. The quantity $D(\boldsymbol{x})$ is the density of the objects at $\boldsymbol{x}$, and $D(\boldsymbol{x})\mathrm{d}\boldsymbol{x}$ is the expected number of objects contained in the infinitesimal region $\mathrm{d}\boldsymbol{x}$. Thus the expected number of objects in a closed region $\mathcal{R}$ is $\int_{\mathcal{R}} D(\boldsymbol{x})\mathrm{d}\boldsymbol{x}$.

Two types of RFSs relevant for this thesis work deserve spatial attention: Bernoulli RFS, and Poisson point process (PPP) RFS. They can be extended to multi-Bernoulli (MB) RFS, multi-Bernoulli mixture (MBM) RFS and combined in a Poisson multi-Bernoulli mixture (PMBM) RFS. These are described below.

5.2.1 Bernoulli RFS

A Bernoulli RFS $\boldsymbol{X}$ has multiobject probability distribution [59]

$$f(\boldsymbol{X}) = \begin{cases} 1 - r, & \boldsymbol{X} = \emptyset, \\ r \cdot f(\boldsymbol{x}), & \boldsymbol{X} = \{\boldsymbol{x}\}, \\ 0, & |\boldsymbol{X}| \geq 2, \end{cases} \tag{5.6}$$

where $r \in [0, 1]$ denotes the probability that a target exists and if a target with state $\boldsymbol{x}$ exists, then $f(\boldsymbol{x})$ is its PDF. The PHD of a Bernoulli RFS is

$$D(\boldsymbol{x}) = r \cdot f(\boldsymbol{x}). \tag{5.7}$$

A multi-Bernoulli (MB) RFS is the union of independent Bernoulli RFSs. A MB is fully parametrized by $\{r_i, f_i(\boldsymbol{x})\}_{i \in \mathbb{I}}$, where $\mathbb{I}$ is its index set. Its multiobject probability

distribution can be expressed as

$$f(\boldsymbol{X}) = \sum_{\uplus_{i\in\mathbb{I}}\boldsymbol{X}_i=\boldsymbol{X}} \prod_{i\in\mathbb{I}} f_i(\boldsymbol{X}_i) \tag{5.8}$$

for $|\boldsymbol{X}| \leq |\mathbb{I}|$, and $f(\boldsymbol{X}) = 0$ otherwise. The notation, $\boldsymbol{X}_1 \uplus \boldsymbol{X}_2 = \boldsymbol{X}$ means $\boldsymbol{X}_1 \cup \boldsymbol{X}_2 = \boldsymbol{X}$ and $\boldsymbol{X}_1 \cap \boldsymbol{X}_2 = \emptyset$. The PHD of a MB RFS is

$$D(\boldsymbol{x}) = \sum_{i\in\mathbb{I}} r_i \cdot f_i(\boldsymbol{x}). \tag{5.9}$$

The multiobject probability distribution of a multi-Bernoulli mixture (MBM) is the normalized, weighted sum of multiobject probability distributions of MBs, which can be stated as [16]

$$f(\boldsymbol{X}) = \sum_{j\in\mathbb{J}} w_j \sum_{\uplus_{i\in\mathbb{I}^j}\boldsymbol{X}_i=\boldsymbol{X}} \prod_{i\in\mathbb{I}^j} f_{j,i}(\boldsymbol{X}_i). \tag{5.10}$$

It is parametrized by $\{w_j, \{r_{j,i}, f_{j,i}(\boldsymbol{x})\}_{i\in\mathbb{I}^j}\}_{j\in\mathbb{J}}$, where w_j is the weight of MB j, and $\mathbb{J}$ is the index set of the MBs in the MBM. An MB is therefore a special case of an MBM with $|\mathbb{J}| = 1$.

5.2.2 Poisson RFS

A PPP, also called Poisson RFS, is a type of RFS, where the cardinality follows a Poisson distribution, and its elements are independent identically distributed (IID). It is parametrized by the intensity function, i.e., the PHD $D(\boldsymbol{x}) = \lambda f(\boldsymbol{x})$, where $\lambda > 0$ is the Poisson rate and $f(\boldsymbol{x})$ is a PDF on the single element state $\boldsymbol{x}$. The multiobject probability distribution of a PPP is [16], [59]

$$f(\boldsymbol{X}) = e^{-\langle D;1\rangle} \prod_{\boldsymbol{x}\in\boldsymbol{X}} D(\boldsymbol{x}), \tag{5.11}$$

where $\langle g, h\rangle = \int g(\boldsymbol{x})h(\boldsymbol{x})\mathrm{d}\boldsymbol{x}$ denotes the inner product.

5.2.3 PMBM RFS

A Poisson multi-Bernoulli mixture (PMBM) RFS is created by the disjoint set union of a PPP and a MBM having multiobject probability distribution [16]

$$f(\boldsymbol{X}) = \sum_{\boldsymbol{X}^u\uplus\boldsymbol{X}^d=\boldsymbol{X}} f^u(\boldsymbol{X}^u) f^d(\boldsymbol{X}^d), \tag{5.12}$$

where $f^u(\cdot)$ has multiobject probability distribution (5.11), and $f^d(\boldsymbol{X}^d)$ has multiobject probability distribution (5.10), where for $|\mathbb{J}| = 1$, (5.12) is called Poisson multi-Bernoulli (PMB).

5.2.4 State Extraction

A common way to extract the set states from a Bernoulli process with RFS density $f(\boldsymbol{X})$ is by comparing the probability of existence r to an existence threshold r_{th}. For $r > r_{\text{th}}$, the state (target) is said to exist and has PDF $f(\boldsymbol{x})$. Its state can then be estimated by the mean $\hat{\boldsymbol{x}} = \int \boldsymbol{x} f(\boldsymbol{x}) \mathrm{d}\boldsymbol{x}$. An estimator to extract the states of a MB is found in a similar fashion, where each Bernoulli component above the existence threshold is reported. State extraction from a MBM is more involved. One possible estimator is to extract only the Bernoulli components of the MB with highest weight. See, e.g., [60], for a detailed discussion on state extraction from MBMs.

5.3 Probability Hypothesis Density Filter

This filter propagates the PHD of the full multiobject posterior distribution $f(\boldsymbol{X}_k|\boldsymbol{Z}_{1:k})$ forward in time [57], [59]. Several implementations of the PHD filter have been proposed based on, e.g., Gaussian mixture models or sequential Monte-Carlo methods [59], [61], [62]. This filter allows to incorporate target appearance and disappearance, as well as clutter measurements. It assumes a standard MTT motion model [57, Ch. 16.3]: (i) motion of individual targets is described by a single target Markov density, (ii) targets appearance is described by the birth PHD and by the spawning (of new targets by existing targets) PHD, and (iii) targets disappear according to IID Markovian processes. Furthermore, the standard MTT measurement model is assumed: (i) false alarm measurements due to clutter are Poisson distributed, (ii) target measurements are independent of each other; at most one measurement is generated per target described by the probability of detection, and (iii) a target generated measurement follows the single-target measurement model. Additionally, the PHD filter assumes that the predicted multiobject probability distribution is Poisson.

The PHD filter propagates the PHD (c.f. Section 5.2) forward in time by alternating prediction and update steps:

$$\ldots \rightarrow D_{k-1|k-1}(\boldsymbol{x}) \rightarrow D_{k|k-1}(\boldsymbol{x}) \rightarrow D_{k|k}(\boldsymbol{x}) \rightarrow \ldots \tag{5.13}$$

Above, $D_{k-1|k-1}(\boldsymbol{x})$ is the prior PHD of $f(\boldsymbol{X}_{k-1}|\boldsymbol{Z}_{1:k-1})$, $D_{k|k-1}(\boldsymbol{x})$ denotes the predicted prior PHD, and $D_{k|k}(\boldsymbol{x})$ denotes the posterior PHD. Propagating only the PHD and the assumption that the multitarget RFS is approximately Poisson, imposes a huge information loss compared to propagating the full multitarget density.

A drawback of the filter is that the uncertainty of the estimated number of targets is high when many targets are present. This deficiency has been addressed in the cardinal-

ized PHD (CPHD) filter, which additionally propagates the cardinality distribution of the estimated number of targets forward in time [57]:

$$\ldots \rightarrow \begin{matrix} D_{k-1|k-1}(\boldsymbol{x}) \\ p_{k-1|k-1}(n) \end{matrix} \rightarrow \begin{matrix} D_{k|k-1}(\boldsymbol{x}) \\ p_{k|k-1}(n) \end{matrix} \rightarrow \begin{matrix} D_{k|k}(\boldsymbol{x}) \\ p_{k|k}(n) \end{matrix} \rightarrow \ldots \tag{5.14}$$

Above, $p_{k-1|k-1}(n)$ denotes the cardinality distribution of $f(\boldsymbol{X}_{k-1}|\boldsymbol{Z}_{1:k-1})$.

5.4 Multi-Bernoulli Filters

Another type of RFS based MTT filters are MB filters which directly approximate the multiobject posterior distribution instead of compressing it into summary statistical moments [59].

The multiple target multi-Bernoulli (MeMBer) filter directly approximates the multiobject posterior distribution by a MB distribution. This filter suffered an estimation bias for the target number due to an ill-considered Taylor expansion in the measurement update step [59]. This was corrected in the cardinality balanced MeMBer (CBMeMBer) filter [63]. This filter propagates the parameters of the posterior MB distribution. Different to the PHD filter, targets do not spawn and target birth is described by a MB distribution. With every measurement, a new target track is introduced causing the number of targets to grow over time. Due to this, track pruning and merging is required to limit computational complexity [59].

A different representation of the multiobject distribution using δ-generalized labelled multi-Bernoullis (δ-GLMBs) enables a closed form solution to the multitarget Bayes recursion (5.1) and (5.2). The drawback of the resulting δ-GLMB filter is that the number of posterior components grows exponentially [64]. A different representation using labeled multi-Bernoullis (LMBs) allows to reduce computational complexity [65]. The resulting LMB filter allows to retrieve the entire trajectory of targets, i.e., the maintenance of track continuity. This comes with a caveat, where in scenarios with track coalescence, the δ-GLMB filter has difficulties with determining the track label of new targets with the result that physically impossible target trajectories are output [66], [67]. An alternative approach to labeled MB filters, where target estimates under the same label are connected to a target trajectory, is by having the whole target trajectory as target state [68], [69]. A trajectory PHD filter and a trajectory PMBM filter was presented in [70] and in [66], respectively.

A representation of the multiobject distribution without labels was presented with the PMBM filter, which represents the posterior multiobject density by the union of a MBM RFS representing detected targets and a Poisson RFS representing unknown targets (targets which are hypothesized to exist but have not yet been detected) [58], [60]. Through the observation that DA implicitly arises in the derivation, it seeks to approximate the discrete distribution of DA. This target representation structure is

more efficient and has a lower computational cost compared to the δ-GLMB/LMB filter [71], [72].

An efficient implementation is achieved with the track-oriented marginal MeMBer/Poisson (TOMB/P) filter, which approximates the joint DA by the product of the marginals similar to JPDA [58]. This approximation can be seen to preserve the first moment of the multiobject posterior distribution. To find the marginal DAs, an efficient FG representation exists, whose solution is found by running the sum-product algorithm (SPA) on a FG [46], [47], c.f. Sec. 4.5. Other approaches for the DA exist as well based on, e.g., variational inference [73]. The TOMB/P filter does not output explicit target tracks, but a track label can be appended to the single target state [58]. A Gaussian mixture implementation of the TOMB/P filter was presented in [58] and a sequential Monte-Carlo implementation was presented in [74].

The measurement-oriented marginal MeMBer/Poisson (MOMB/P) filter is closely related to the TOMB/P filter, but where first hypotheses are expressed over the measurements instead of the target tracks and then the joint association probability is approximated by the marginal association PDFs [58]. Furthermore, in [73] a variational approximation of the MBM resulting after the measurement update step was proposed for the PMBM filter, which shows improved performance compared to TOMB/P and MOMB/P filters when target tracks are spatially close.

5.4.1 PMBM Filter

Here, we outline the PMBM filter from [58]. The filter distinguishes from targets which have at least been detected once (via a measurement) and unknown targets (targets which are hypothesized to exist but have not yet been detected). This allows to split the target RFS into two disjoint subsets representing the two types of targets, i.e.,

$$\boldsymbol{X} = \boldsymbol{X}^u \uplus \boldsymbol{X}^d, \tag{5.15}$$

where $\boldsymbol{X}^u$ represents unknown targets and $\boldsymbol{X}^d$ represents detected targets. The PMBM filter is realized under the following assumptions on the target state and measurement models [58]. Assumptions on the target dynamics:

- new targets arrive according to a non-homogeneous PPP with birth intensity $D(\boldsymbol{x})$,
- targets survive in state $\boldsymbol{x}$ with probability $p_{\mathrm{S}}(\boldsymbol{x})$, and
- target motion follows IID Markovian processes with single target PDF $p(\boldsymbol{x}_k|\boldsymbol{x}_{k-1})$.

Furthermore, is has the following assumptions on the measurement model:

- each target generates at most one measurement per time step with detection probability $p_{\mathrm{D}}(\boldsymbol{x})$,
- a single measurement belongs to at most one target,

- false alarm measurements arrive according to a non-homogeneous PPP with intensity $\kappa(\boldsymbol{z})$ and are independent of target generated measurements, and
- each target generated measurement is independent of other measurements and has single target measurement likelihood $p(\boldsymbol{z}|\boldsymbol{x})$.

Additionally, to the assumptions on the target dynamics and the measurement model, the following hypotheses are defined [58]:

- A single target hypothesis is a subset of measurements that are hypothesized to be originated from to the same potential target.
- A track contains information about a certain target consisting of single target hypotheses. It is initiated by the first measurement detecting the target.
- A global hypothesis $j \in \mathbb{J}$ is a choice of single target hypotheses, one for each track. Here, $\mathbb{J}$ is the index set of global association history hypotheses.
- A valid global hypothesis is a global hypothesis, where in each time step each measurement has been assigned to a track exactly once.

The assumptions and definitions above allow to model the target density by a combination of a PPP representing the undetected targets and a MBM for the detected targets, consisting of a weighted MB for each global hypothesis. Hence, the prior target density can be stated as the PMBM

$$f(\boldsymbol{X}_{k-1}|\boldsymbol{Z}_{1:k-1}) = \sum_{\boldsymbol{X}^u \uplus \boldsymbol{X}^d = \boldsymbol{X}_{k-1}} f^u(\boldsymbol{X}^u) f^d(\boldsymbol{X}^d), \tag{5.16}$$

where $f^u(\cdot)$ is a Poisson RFS defined in (5.11) and $f^d(\cdot)$ is a MBM defined in (5.10). The PMBM at time $k-1$ is described by the parameters

$$\{w_{k-1,j,i}, r_{k-1,j,i}, f_{k-1,j,i}(\cdot)\}_{i \in \mathbb{I}_{k-1,j}, j \in \mathbb{J}_{k-1}}. \tag{5.17}$$

The single target hypotheses $w_{k-1,j,i}$ are related to the global hypothesis by

$$w_{k-1,j} \propto \prod_{i \in \mathbb{I}_{k-1,j}} w_{k-1,j,i} \tag{5.18}$$

for all $j \in \mathbb{J}_{k-1}$ (c.f. (5.12)), where $\sum_{j \in \mathbb{J}_{k-1}} w_{k-1,j} = 1$.

The filter consists of alternating prediction and update steps retaining the independent PMBM form of the posterior density. In the update step, a new (target) track is created for each measurement in $\boldsymbol{Z}_k$ by updating the PPP by the measurement. Furthermore, the MBM is updated containing single target hypotheses for detection by each measurement in $\boldsymbol{Z}_k$, a miss detection, and that the target does not exist. As time progresses, the

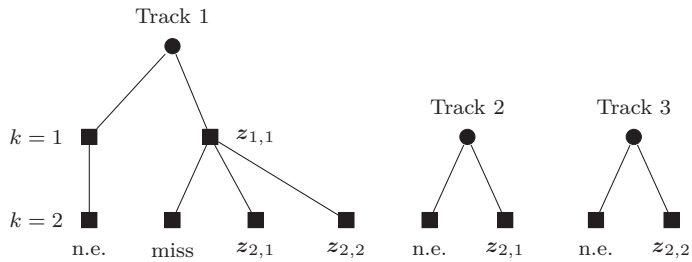

Figure 5.1. Illustration of single target hypothesis trees maintained by the PMBM filter. In this example, there is initially no target present. At time $k = 1$, measurement $\boldsymbol{Z}_1 = \{\boldsymbol{z}_{1,1}\}$ is received and a new track (Track 1) is initiated. There is a hypothesis for $\boldsymbol{z}_{1,1}$ to Track 1, and a hypothesis that the track does not exist (n.e.). At time $k = 2$, two measurements $\boldsymbol{Z}_2 = \{\boldsymbol{z}_{2,1}, \boldsymbol{z}_{2,2}\}$ are received. Each measurement may be the source of a new target and therefore new tracks are initiated (Track 2, Track 3). For each of the already existing tracks, a new hypothesis for each measurement is added. Additionally, the existing targets might not have produced a measurement at the current time step and a miss detection hypothesis is added (miss).

number of tracks and the hypothesis tree of each track increase. An example of the hypotheses trees maintained by the PMBM filter is illustrated in Fig. 5.1.

The single hypothesis weights of each track are recursively updated depending on the association. A missed detection hypothesis of an existing track $i \in \mathbb{I}_{k,j}$ with hypothesis weight $w_{k-1,j,i}$, has an updated weight [58]

$$w_{k,j,i} = w_{k-1,j,i} \left(1 - r_{k|k-1,j,i} + r_{k|k-1,j,i} \left\langle f_{k|k-1,j,i}, 1 - p_{\mathrm{D}} \right\rangle\right), \tag{5.19}$$

where $r_{k|k-1,j,i}$ denotes the predicted probability of existence of Bernoulli component $i \in \mathbb{I}_{k,j}$ under global hypothesis $j \in \mathbb{J}_k$, and $f_{k|k-1,j,i}(\boldsymbol{x})$ is the predicted state PDF. The weight considers the two cases of non-existence and non-detection of the target in the predicted state. A measurement update hypothesis of an existing track $i \in \mathbb{I}_{k,j}$ with hypothesis weight $w_{k-1,j,i}$ by measurement $\boldsymbol{z} \in \boldsymbol{Z}_k$, has an updated weight [58]

$$w_{k,j,i} = w_{k-1,j,i} r_{k|k-1,j,i} \left\langle f_{k|k-1,j,i}, p(\boldsymbol{z}|\cdot) p_{\mathrm{D}} \right\rangle \tag{5.20}$$

considering the case of detection in the current state under the measurement model $p(\boldsymbol{z}|\boldsymbol{x})$. A new track denoted i, is initialized for measurement $\boldsymbol{z} \in \boldsymbol{Z}_k$, and the set of tracks is extended $\mathbb{I}_{k,j} = \mathbb{I}_{k-1,j} \cup i$. This single hypothesis has weight [58]

$$w_{k,j,i} = \kappa(\boldsymbol{z}) + \langle D_+, p(\boldsymbol{z}|\cdot) p_{\mathrm{D}} \rangle \tag{5.21}$$

considering the two cases of a false alarm according to the clutter model with inten-

sity $\kappa(\boldsymbol{z})$ and a new detection according to the undetected target model with predicted intensity denoted $D_+(\boldsymbol{x})$.

In principle, we could update each target track by new hypotheses for non-detection, miss, and detection by one of the measurements. This procedure results in non-valid global hypotheses, where the assumptions on the measurement model does not hold, i.e., double usage of a single measurement for updating different target tracks. In order to achieve a tractable implementation, non-valid global hypotheses as well as unlikely hypotheses (hypotheses with a negligible weight) should not be maintained by the filter. The TOMB/P filter presented next provides a tractable implementation of the PMBM filter by maintaining only a single valid global hypothesis.

5.4.2 TOMB/P Filter

The TOMB/P filter assumes the prior density of form PMB, i.e., the MBM representing the detected targets contains only a single MB with weight one [58]. The filter then seeks an approximation of the MBM resulting after the update step by a single MB. The global hypothesis weight (5.18) is equal to the PDF of joint association

$$w_j = p(w_{j,1}, \ldots, w_{j,n}), \tag{5.22}$$

where we omitted the time index for brevity and $w_{j,i}$ denotes the single target hypotheses for $i \in \mathbb{I}$ with $|\mathbb{I}| = n$. Since it is difficult to compute the joint association PDF, it is approximated by the product of marginal PDFs with [58]

$$p(w_{j,1}, \ldots, w_{j,n}) \approx \prod_{i \in \mathbb{I}} \int \cdots \int p(w_{j,1}, \ldots, w_{j,n}) \mathrm{d}w_{j,1} \mathrm{d}w_{j,i-1} \mathrm{d}w_{j,i+1} \mathrm{d}w_{j,n}. \tag{5.23}$$

An efficient method to obtain approximate marginal PDFs is by running the SPA on a FG, where the single hypothesis weights $w_{k,j,i}$ are input [46], [47]. The FG is constructed in a way such that non-valid global hypotheses are avoided similar (c.f. Sec. 4.5). With the marginal PDFs at hand, the updated PMBM of form (5.16) can be easily reduced to a PMB ensuring the posterior density is in the same form as the prior. In doing so, the hypothesis trees of each target track are pruned to contain only a single valid global hypothesis, with the result that $w_{k|k-1,j,i} = 1, \forall i, j$ in (5.19) and (5.20).

5.5 Uncertain Sensor State

The uncertain sensor state can be incorporated in the Bayesian filtering framework similar to the random vector (RV) case (c.f. Sec. 4.4). The posterior (5.2) is then formulated on the joint state $\boldsymbol{X}_k, \boldsymbol{x}_k$, where $\boldsymbol{X}_k$ denotes the target RFS and $\boldsymbol{x}_k$ denotes the sensor

state, written as

$$f(\boldsymbol{X}_k, \boldsymbol{x}_k|\boldsymbol{Z}_{1:k}) = \frac{f(\boldsymbol{Z}_k|\boldsymbol{X}_k, \boldsymbol{x}_k) f(\boldsymbol{X}_k, \boldsymbol{x}_k|\boldsymbol{Z}_{1:k-1})}{\iint f(\boldsymbol{Z}_k|\boldsymbol{X}_k, \boldsymbol{x}_k) f(\boldsymbol{X}_k, \boldsymbol{x}_k|\boldsymbol{Z}_{1:k-1}) \delta\boldsymbol{X}_k \mathrm{d}\boldsymbol{x}_k}. \tag{5.24}$$

In [38] and [75], a modification of the PHD filter was proposed to estimate an unknown sensor bias. In [76], a Bernoulli filter was proposed to incorporate sensor uncertainty.

Approaches based on Rao-Blackwellization for the simultaneous localization and mapping (SLAM) problem have also been proposed, where many of these methods track the sensor state via a particle filter and estimate the targets (landmarks) using a conventional MTT filter; one filter for each sensor particle (see e.g., [77]–[79]).

Since the joint posterior density (5.24) is difficult to compute, one can proceed and approximate it, in the minimum Kullback-Leibler divergence (KLD) sense, by the marginal densities of the sensor/target states. Then,

$$\begin{aligned} f(\boldsymbol{X}_k, \boldsymbol{x}_k|\boldsymbol{Z}_{1:k}) =& f(\boldsymbol{X}_k|\boldsymbol{x}_k, \boldsymbol{Z}_{1:k}) p(\boldsymbol{x}_k|\boldsymbol{Z}_{1:k}) && (5.25) \\ \approx& f(\boldsymbol{X}_k|\boldsymbol{Z}_{1:k}) p(\boldsymbol{x}_k|\boldsymbol{Z}_{1:k}), && (5.26) \end{aligned}$$

where the equality is due to the product rule and the marginal densities are obtained by

$$f(\boldsymbol{X}_k|\boldsymbol{Z}_{1:k}) = \int f(\boldsymbol{X}_k, \boldsymbol{x}_k|\boldsymbol{Z}_{1:k}) \mathrm{d}\boldsymbol{x}_k, \tag{5.27}$$

$$p(\boldsymbol{x}_k|\boldsymbol{Z}_{1:k}) = \int f(\boldsymbol{X}_k, \boldsymbol{x}_k|\boldsymbol{Z}_{1:k}) \delta\boldsymbol{X}_k. \tag{5.28}$$

Note that [40], [80] reported for the SLAM problem that the partitioning of sensor and landmark posterior as done in (5.26) generates optimistic estimates about the state uncertainty.

Direct calculation of the marginal densities in this way can be involved due to the structure of the joint posterior density $f(\boldsymbol{X}_k, \boldsymbol{x}_k|\boldsymbol{Z}_{1:k})$. In Paper D and E, we obtain the marginal densities of the sensor/target states approximately. The result is a low complexity PMBM based filter for joint sensor-target state tracking. The benefit of this approach is that existing MTT frameworks can be employed for target tracking in scenarios involving an uncertain sensor state. Additionally, target measurements provide information to update the sensor state. In a multi-sensor setup using the iterator-corrector approach, this means that sensor state uncertainty is reduced when target measurements are accurate and when the prior on the targets is high.

5.6 Extended Target Tracking

MTT filters rely on the point target assumption. This is a reasonable assumption when the sensor resolution is low w.r.t. the size of the target, which is, e.g., the case for surveil-

lance of the sky with ground-to-air radars. On the other hand, in an intelligent transportation system (ITS) the sensor resolution is high w.r.t. the object size. For instance, an autonomous driving car equipped with a lidar sensor obtains in one measurement scan multiple reflections from a single road user (e.g., a car or a cyclist). Then the target extent needs to be modeled and possibly estimated as well, leading to an extended target tracking (ETT) filter.

In ETT, each target with extent denoted ET gives rise to possibly multiple detections, its shape can be a priori unknown and may change over time, and the objective is to estimate the ET's kinematic state as well the extent [14]. A related objective may be found in computer vision, where multiple objects need to be estimated from single images or a sequence of images, with the difference that the camera provides a rich view of the environment. In contrast, in ETT the ET's state and extent can seldom be estimated in a single time step due to the sparsity of the sensor measurements. Depending on the application, an ET might be a car, a pedestrian, a cyclist, etc.: a rigid body model can be assumed. Related to ETT is group object tracking, where instead of a single entity a group of entities is tracked. For instance a group of pedestrians walking on the sideway. In such an application, the rigid body model may not be applicable.

Several ETT filters have been developed, often as extensions of their point target counterparts. For a comprehensive overview of works on ETT see [14].

5.6.1 Measurement Models for the Extent of a Single Target

In [14], several measurement models for the target extent are identified in literature, where we depict here two of them.

Points on a Rigid Body Model

In the set of points on a rigid body (SPRB) model, the target shape is assumed to be known and reflection points along the surface are identified. It is assumed that each reflection point l generates a measurement with probability of detection p_{D}^{l}. The measurement likelihood for measurement set $\boldsymbol{Z} = \{\boldsymbol{z}_1, \ldots, \boldsymbol{z}_m\}$ and L reflection points is [14]

$$p(\boldsymbol{Z}|\boldsymbol{x}) = \begin{cases} \sum_{\boldsymbol{a}} \prod_{a_l=0} (1 - p_{\mathrm{D}}^{l}) \prod_{a_l>0} p_{\mathrm{D}}^{l} p_l(\boldsymbol{z}_{a_l}|\boldsymbol{x}), & |\boldsymbol{Z}| \leq L, \\ 0, & \text{otherwise.} \end{cases} \tag{5.29}$$

Here, $p_l(\boldsymbol{z}_{a_l}|\boldsymbol{x})$ is the measurement model w.r.t. the l-th reflection point using measurement $\boldsymbol{z}_{a_l}$, and $\boldsymbol{a} = [a_1, \ldots, a_L]^{\mathsf{T}}$ is an assignment variable with a_l assigning the l-th reflection point to measurement $\boldsymbol{z}_{a_l}$. This model requires a DA routine for measurements originated from the same ET, which can be computational demanding for a high number of reflection points.

Spatial Model

Different to the SPRB model, the spatial model defines a spatial density from which the measurements are generated. This model is continuous in which parts of the target can generate measurements.

Often, a non-homogeneous PPP is used to model target generated measurements with measurement rate $\gamma(\boldsymbol{x})$. The detection probability is in this model spatially represented due to the dependency of the measurement rate on the target state. The measurement likelihood is [14]

$$p(\boldsymbol{Z}|\boldsymbol{x}) = e^{-\gamma(\boldsymbol{x})}\gamma(\boldsymbol{x})^{|\boldsymbol{Z}|} \prod_{\boldsymbol{z}\in\boldsymbol{Z}} p(\boldsymbol{z}|\boldsymbol{x}). \tag{5.30}$$

The benefit of this model is that it avoids DA to reflection points on the object. It does not avoid the multi-object DA. This model has been used in ETT, where each ET state is augmented by the measurement rate γ allowing to estimate the rate for each target individually [16], [81]. This model is also used in Paper F.

Note that the SPRB model and the spatial model can also be combined. In [82], [83], the SPRB model is used to describe reflection points on a vehicle when observed by an automotive radar. This was then combined with the spatial model to handle uncertainty w.r.t. the reflection points due to the limited sensor resolution.

5.6.2 Models for the Shape of a Single Target

Different models for the ET's extent exist in ETT, reaching from not modeling the extent at all, to assuming a specific geometric shape with, e.g., unknown translation and rotation, to non-parametric models to describe, e.g., star-convex objects. Typically, more complex models provide a richer shape description. Two popular models are the random matrix (RM) model [84], where the target shape is described by an ellipsoid; and a non-parametric Gaussian process (GP) model approach [30], where a star convex-target extent is described by a GP.

In the following, we describe measurement models for the star-convex shape model. Note that a set $\mathcal{S}$ is star-convex if all possible line segments from the center to any point in $\mathcal{S}$ are in the set. The target surface measurement model is [14]

$$\boldsymbol{z} = s \cdot r(\boldsymbol{p}, \phi) + \boldsymbol{c} + \boldsymbol{n}, \tag{5.31}$$

where $r(\boldsymbol{p}, \phi)$ denotes the radius function with input parameter vector $\boldsymbol{p}$ and angle ϕ, $\boldsymbol{c}$ denotes the ET center, s is multiplicative noise between zero and one specifying the relative distance between $\boldsymbol{c}$ and the target contour, and $\boldsymbol{n}$ is the additive measurement noise. A variation of this model is the target contour model, where measurements solely originate from the target's contour. Hence, the noise term s in (5.31) is not present [30].

The radius function for the shape contour can be defined via a Fourier series expansion

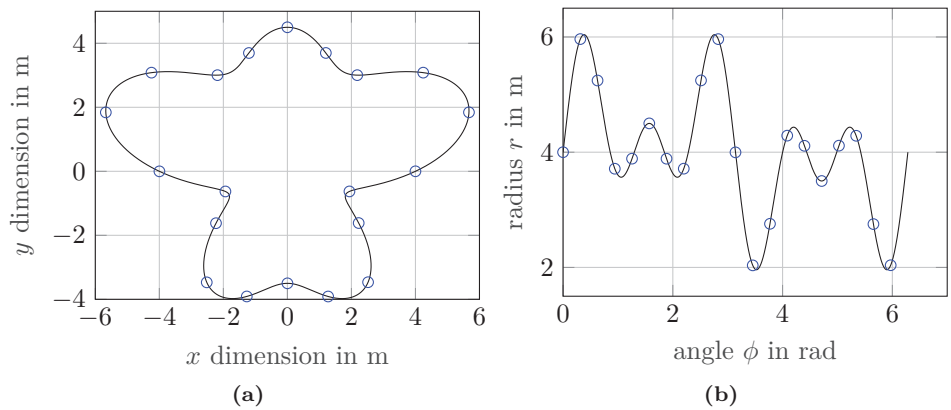

Figure 5.2. Example of a star-convex object in Cartesian and polar coordinate system.

and for Bayesian state estimation a non-linear Kalman filter (KF) can be employed [14]. Thereby, a higher number of Fourier components allows to encode more details about the target contour.

Also GPs have been used to describe the target extent. In doing so, the radius function is assumed to follow a real stochastic process, which can be modeled by a GP. In [30], a GP with input angle ϕ is used to model the target contour, i.e.,

$$s \cdot r(\boldsymbol{p}, \phi) = f(\phi), \tag{5.32}$$

$$f(\phi) \sim \mathcal{GP}(\mu(\phi), k(\phi, \phi')), \tag{5.33}$$

where $\mu(\cdot)$ denotes the mean function and $k(\cdot, \cdot)$ is the kernel function (see also Sec. 3.4). A GP model has the benefit that uncertainty about the non-linear function (target contour) is naturally encoded. To allow for a Bayesian estimation on the target contour, recursive GP regression is employed. This means that instead of conditioning on all measurements $\boldsymbol{z}_{1:k}$ with inputs $\phi_{1:k}$ (the database), a database with a fixed number of inputs (basis points) $\tilde{\boldsymbol{\phi}} = [\tilde{\phi}_1, \ldots, \tilde{\phi}_N]^\mathsf{T}$ and corresponding outputs $\boldsymbol{f} = [f(\tilde{\phi}_1), \ldots, f(\tilde{\phi}_N)]^\mathsf{T}$ is used. Fig. 5.2a and Fig. 5.2b show an example of a star-convex target shape in Cartesian and polar coordinate system, respectively. Additionally, $N = 20$ basis points are shown. In [30], the approach of [85] was used, where the posterior distribution $p(\boldsymbol{f}|\boldsymbol{z}_{1:k})$ is updated sequentially. The posterior PDF on $\boldsymbol{f}$ becomes [30]

$$p(\boldsymbol{f}|\boldsymbol{z}_{1:k}) \propto p(\boldsymbol{z}_k|\boldsymbol{f}, \boldsymbol{z}_{1:k-1}) p(\boldsymbol{f}|\boldsymbol{z}_{1:k-1}). \tag{5.34}$$

To ensure that the database size remains constant, old measurements are discarded

leading to

$$p(\boldsymbol{z}_k|\boldsymbol{f}, \boldsymbol{z}_{1:k-1}) \approx p(\boldsymbol{z}_k|\boldsymbol{f}). \tag{5.35}$$

It is therefore assumed that the posterior on $\boldsymbol{f}$ (with inputs $\tilde{\boldsymbol{\phi}}$ potentially different to $\phi_{1:k}$) contains sufficient information to encode the target extent, which may be a reasonable assumption for a sufficient number of basis points.

With the help of a KF, the posterior (5.34) can be updated for the case the hyper-parameter values are known, and under certain restrictive assumptions the hyper-parameter values can be estimated inside KF [85]. The GP model has the benefit that a prior target shape is defined, which is updated as target measurements arrive. This allows also to incorporate targets with changing shapes.

The GP model is used for tracking a single ET with the help of a KF in [30], [86] and using a particle filter in [87]. For tracking multiple ETs using a LMB filter in [88] and in Paper F using a PMB filter.

5.6.3 Data Association

Since an ET can give rise to multiple measurements, the point target assumption made in MTT filters, that a target generates at most one measurement per sensor and time step, becomes invalid. Compared to point targets, DA with ET becomes much more involved due to the increased number of possible partitions of the measurement set $\boldsymbol{Z}$ into subsets of measurements from the same source and associations w.r.t. the source. The number of possible partitions is described by the Bell number which grows rapidly with the size of $\boldsymbol{Z}$ [14]. In Bayesian optimal filtering, all possible partitions and associations have to be considered. A tractable ETT filter implementation needs to resort to complexity reduction mechanisms such as, e.g., distance based clustering and gating.

As an example, consider the scenario outlined in Fig. 5.3, where there are two ETs present. The number of possible partitions for $|\boldsymbol{Z}| = 36$ is $3.8{\cdot}10^{30}$. Under the assumption that ETs are non-overlapping in space, a distance based clustering method may produce the partitioning into four cells indicated by the color of the measurements. Using this partition, DA becomes tractable.

Note that depending on the measurement model for the ET an additional DA step with measurements belonging to the same target is needed. For instance, in the SPRB model, the association of a measurement w.r.t. the reflection point need to be resolved (c.f. Sec. 5.6.1).

5.7 Information Fusion

Similar to the RV case discussed in Section 4.6, two types of information fusion can be distinguished: likelihood fusion, and posterior fusion.

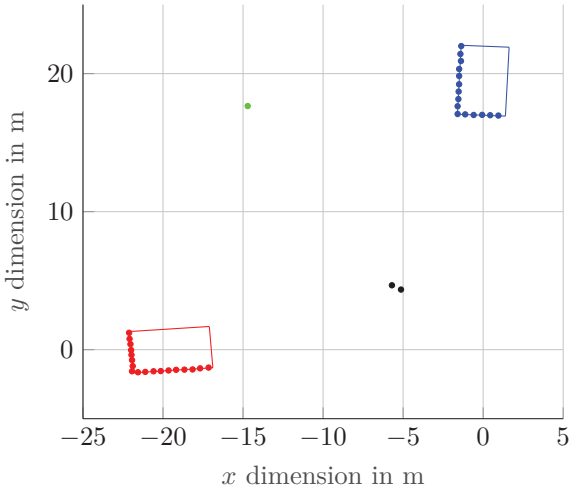

Figure 5.3. Measurement partitioning of measurement set $\boldsymbol{Z}$. Measurements are plotted as dots, where the color indicates the partitioning.

5.7.1 Likelihood Fusion

Likelihood fusion refers to the case where there is a single filter and multiple sensors present (c.f. Fig. 4.4). The measurement set provided by each sensor is denoted as $\boldsymbol{Z}_{s,k}$ with $s = 1, \ldots, N$. We are interested in calculating the multitarget posterior density $p(\boldsymbol{X}_k | \boldsymbol{Z}_{1,1:k}, \ldots, \boldsymbol{Z}_{N,1:k})$. With similar reasoning as in the RV case, the set measurement likelihood in (5.2) becomes

$$p(\boldsymbol{Z}_k | \boldsymbol{X}_k) = p(\boldsymbol{Z}_{1,k}, \ldots, \boldsymbol{Z}_{N,k} | \boldsymbol{X}_k). \tag{5.36}$$

In [59], it was pointed out for the PHD filter that the incorporation of multiple sensors is computationally problematic due to the partitions of the measurement set. To avoid this, a heuristic approach is found by applying the update step sequentially for each sensor called the iterator-corrector approach. Furthermore with this approach, the order of which measurement set is used in the sequential update steps produces different numerical results when the detection probabilities of the sensors are significantly different. Then the sensor with a higher detection probability should be used first. For similar detection probabilities no significant difference is seen. In Papers E and F, we perform the iterator-corrector approach to compute the posterior (5.2) in a multi-sensor setup.

5.7.2 Posterior Fusion

Similar to the RV case, a suboptimal fusion of posterior information can be performed when correlation is unknown. In [52], a generalization for robust fusion of multiobject

posterior distributions, the generalized covariance intersection (CI) (GCI), also called exponential mixture density (EMD) in some literature, is proposed. The fused multiobject posterior is defined as

$$f_\omega(\boldsymbol{X}_k|\boldsymbol{Z}_{1,1:k},\boldsymbol{Z}_{2,1:k}) = \frac{f_1(\boldsymbol{X}_k|\boldsymbol{Z}_{1,1:k})^\omega f_2(\boldsymbol{X}_k|\boldsymbol{Z}_{2,1:k})^{1-\omega}}{\int f_1(\boldsymbol{X}_k|\boldsymbol{Z}_{1,1:k})^\omega f_2(\boldsymbol{X}_k|\boldsymbol{Z}_{2,1:k})^{1-\omega}\delta\boldsymbol{X}_k}, \tag{5.37}$$

where $\omega \in [0,1]$ is a weighting parameter. Here, $f_i(\boldsymbol{X}_k|\boldsymbol{Z}_{1,1:k})$ is the multiobject posterior distribution for filter $i \in \{1,2\}$. In [89], it was shown that the result of the GCI is also the solution to the Kullback-Leibler average (KLA) for multiobject probability distributions. The KLA for the multiobject probability distributions $f_i(\boldsymbol{X})$ and $i \in \{1,2\}$ is defined

$$f_\omega = \arg\min_f(\omega D(f\|f_1) + (1-\omega)D(f\|f_2)), \tag{5.38}$$

where

$$D(f\|f_i) = \int f(\boldsymbol{X}) \log \frac{f(\boldsymbol{X})}{f_i(\boldsymbol{X})}\delta\boldsymbol{X} \tag{5.39}$$

denotes the KLD extended to multitarget RFS densities [89]. In [90], GCI was demonstrated for Bernoulli RFSs, Poisson RFSs, and cluster RFSs, and in [91] for MB RFSs. In [89], a distributed CPHD filter, and in [91] a distributed MB filter has been developed based on GCI. In Paper F, we utilize GCI to realize a decentralized PMBM filter.

5.8 Summary

Exact Bayesian filtering with RFSs is intractable and we need to resort to approximate methods. Several MTT filters have been proposed in literature, with various degrees of approximations involved. In Papers D and E, we propose a PMBM filter for joint sensor-target state tracking allowing to incorporate uncertainty of the sensor state.

When the size of a target is non-neglible w.r.t. the sensor resolution, the point target assumption made in MTT filters is invalid. An ETT filter models additionally the extent of the target allowing to consider multiple measurements per target at the price of a higher complexity in DA.

Furthermore, we observed that information fusion with RFSs is performed similar the RV case, but where now the full multiobject probability distribution needs to be considered. A suboptimal approach for posterior fusion with unknown correlation can be found by minimizing the KLA of the multiobject posterior distributions collected by independent filters.

In Paper F, we describe the star-convex extent of a target by a GP and incorporate this in an ETT filter. Additionally to this, we propose a decentralized ETT filter through robust fusion of posterior information.

CHAPTER 6

Scientific Achievements, Conclusions and Outlook

This thesis studies problems and proposes solutions within the field of communications and target tracking for multi-agent system (MAS). The contributions of this thesis include:

- channel gain prediction between mobile agents in the presence of location uncertainty,
- a multitarget tracking (MTT) filter for joint target-sensor state tracking,
- a decentralized extended target tracking (ETT) filter for tracking extended targets (ETs) with star-convex shapes.

In Part II, the author's contributions of this thesis in terms of publications are presented. In the following, we state a summary of the scientific achievements, conclusions and possible avenues for future work of this thesis' work.

6.1 Channel Prediction with Location Uncertainty for Multi-Agent Systems (Papers A and B)

Having an accurate channel prediction framework is imperative for reliable wireless communications, which is required by future applications such as remote-controlled driving or when an autonomous vehicle should make decisions based on information acquired by a different agent. In achieving this, the positions of the transmitter (TX) and re-

ceiver (RX), as well as the environment, need to be known and any uncertainties need to be accounted for.

In Papers A and B, we proposed to model the average received power by a Gaussian process (GP) model. This model allows to incorporate any present location uncertainty of the TX and RX in the learning process of the underlying channel parameters (deterministic path-loss and spatial correlation of large-scale fading) from a database of measurements. This also applies to the prediction process, where the predictive distribution of the received power at an arbitrary location is available as closed form expressions for the mean and variance.

For the learning process, this means that the proposed framework produces stable estimates of the channel parameters, independent of the present location uncertainty of the TX and RX associated with the measurement. We applied the proposed channel prediction framework in a MAS scenario with the goal to minimize the end-to-end bit error rate (BER) along a communication path involving multiple agents with different levels of location uncertainty. Based on the predicted channel quality, agents move to optimal locations and the end-to-end BER is evaluated. Since the proposed framework considers the location uncertainty of the agents in the predictive distribution of the average received power, the predicted BER and the BER evaluated at the true agent locations agree well. This resulted in a lower average BER compared to the case of ignoring the agent's location uncertainty.

Possible Extensions

The proposed channel prediction framework does not yet consider variations of the channel caused by multipath, whose incorporation could be a possible extension of this work. Furthermore, the prediction quality depends on the number of data points and their corresponding location uncertainty. To have a computational efficient implementation, allowing to model large environments, it is necessary to limit the number of entries in the database. Approximate methods, such as conditioning on a fixed number of basis points should be considered (c.f [92], [93]).

6.2 Multitarget Tracking with Uncertain Sensor State (Papers C, D and E)

To enable safe and efficient autonomous driving in an urban environment, accurate knowledge of the vehicle's position, as well as of other road users is needed. On one hand, this is enabled by having highly accurate on-board sensors and on the other hand, through fusion of information collected by other vehicles.

In Paper C, we proposed a Bayesian filtering formulation to jointly track the positions of multiple cooperative vehicles and of observed moving targets (called features in this work). In doing so, measurements from two kinds of sensors were utilized: a Global

Positioning System (GPS)-like sensor to obtain the vehicles absolute position, and a radar-like sensor to obtain the relative positions of targets. The radar-sensors' peculiarity of an unknown target-to-measurement association, was incorporated in the factor graph (FG) formulation and the minimum mean square error (MMSE) estimate was found by running nonparametric belief propagation (BP).

When multiple vehicle with different location uncertainties observe the same set of targets, the positioning quality of vehicles with uncertain location can be improved by target tracking. Furthermore, we saw that the accuracy of the target measurements determines how much global information can be transferred from a well localized vehicle to vehicles with lower accuracy by means of target tracking. Thereby, the number of observed targets has an impact on the amount of information which can be transferred between the vehicles within one time step. It is interesting to point out that well-localized vehicles do not benefit by target tracking. The reason for this is simply that no new information in terms of a measurement of an absolute coordinate/position is introduced.

In Paper D and E, we followed a different path to tackle this tracking problem, where we proposed a multisensor Poisson multi-Bernoulli filter for joint target and vehicle state tracking. To enable the usage of standard MTT frameworks, and to achieve a tractable implementation, we performed an approximation of the joint posterior density by minimizing the Kullback-Leibler divergence (KLD). This allowed to maintain an independent structure of the vehicle and of the target state densities. The result of this approach is that a standard Poisson multi-Bernoulli mixture (PMBM) MTT filter can be applied for target tracking, with the modification that the single target likelihood considers the present vehicle (sensor) uncertainty. Furthermore, due to the symmetry in the approximations, an update of the sensor state is possible by means of target tracking.

In a single vehicle scenario, the vehicle's location uncertainty is incorporated in the MTT filter, which allows to produce stable target estimates compared to the case when this uncertainty is ignored (c.f. Paper E). We observed that in terms of target tracking performance, the vehicle state should not be updated by the target measurements. The reason for this is that after the measurement update step, target and vehicle states become correlated, which is not modeled by the proposed filter.

In a multiple vehicle scenario, target measurements from vehicles with different location uncertainties are incorporated sequentially utilizing an iterator-corrector approach. This allows not only accurate target tracking, but also to convey information from targets to vehicles, with the result of an improved position quality compared to the case of vehicle state tracking alone. We demonstrated this not only in simulations but also in an experiment involving real vehicles. Furthermore, we observed that vehicles with high location uncertainty can improve their positioning quality by target tracking only when the observed target set intersected with the target set of observed by vehicles with low location uncertainty is non-empty.

Possible Extensions

The proposed approach of Paper C neither considers target appearance and disappearance nor non-overlapping field-of-views (FoVs) of the radar-like sensors. A natural extension would be to consider them. Note that target appearance and disappearance was addressed in [48], [53]. Furthermore, prior knowledge of the measurement-to-target correspondence, if available, could be incorporated in the FG for the radar-like sensor.

The implementation of the proposed MTT filter of Paper D and E utilizes linear dynamical and measurement models. An extension of this work could consider nonlinear models, e.g., through a sequential Monte-Carlo implementation, thus allowing to model the vehicles orientation. Furthermore, no target labels are maintained by the proposed filter implementation and therefore there are no trajectories for individual targets available. Labels can be added as discussed in [58] or alternative descriptions of the multi-Bernoulli mixture (MBM) filter should be considered when the target tracks are of interest (c.f. Sec. 5.4). The problem of MTT from a vehicle with uncertain location can also be cast as a simultaneous localization and mapping (SLAM) problem, where the whole vehicle trajectory and not only the current vehicle state is of interest. Accordingly, the multi-vehicle scenario would then result in a cooperative SLAM problem. Furthermore, the proposed filter is a centralized approach, which is not desirable for autonomous driving scenarios. The filter could also be extended to that effect allowing to address issues like time synchronization among different vehicles and dealing with the error prone wireless communication channel.

6.3 Decentralized Extended Target Tracking (Paper F)

In Paper F, we adapted a state-of-the art ETT filter to track targets with star-convex shape. Thereby, a GP was used to model the target shape. The ETT filter, together with the GP target shape model, enables to accurately estimate and track the shape and kinematic state of multiple ETs from target contour measurements, where the filter's posterior is modeled by a Poisson multi-Bernoulli (PMB).

We proposed a method to fuse posterior information from multiple independent ETT filters in a way such that the fused density does not underestimate the true uncertainty of the targets (robust fusion). In doing so, fusing the multitarget posteriors was performed separately by fusion of the Poisson random finite sets (RFSs) describing the hypothesized, but not yet detected targets, and by fusing the multi-Bernoulli (MB) RFSs modeling the detected targets. Through utilization of a map for individual Bernoulli components between the MB RFSs, which is described in the minimum KLD sense and found by solving a linear assignment problem, complexity in the fusion step is reduced. After the fusion step, the obtained multitarget posterior can be utilized as a prior density for the independent filters in the next time step.

We observed in simulations that the ETT filter adapted with the GP target shape

model allows to accurately estimate and track multiple extended targets. Furthermore, the filter keeps track of the number of measurements produced by an ET. We observed that incorporation of measurements obtained by multiple sensors using an iterator-corrector approach leads to a distortion of the estimated number of measurements produced by an ET. The reason for this is that this quantity depends also on the sensor configuration with respect to (w.r.t.) the target and not only on the target as modeled by the filter. Notwithstanding that, the ETT tracking error is reduced compared to the single measurement sensor scenario.

In a scenario with multiple independent ETT filters, the proposed posterior fusion can be applied. We observed that the performance is lower than with the centralized approach using an iterator-corrector approach, but higher than using independent ETT filters alone. Furthermore, we observed that fusing of posterior information from more than two posteriors resulted in only small performance gains in the considered scenario. The proposed ETT filter and the proposed fusion method can operate at different rates, which is relevant in capacity limited communication channels. We observed that a higher rate of posterior fusion leads to a higher tracking performance. This means that depending on the application and available communication channel, the rate of the fusion operation can be adapted to meet the required tracking accuracy.

Possible Extensions

The adapted filter reduces the resulting PMBM to a PMB after each measurement update step. This reduction is equivalent with truncation of the hypothesis tree to a single global hypothesis. For posterior fusion, we assumed that the multitarget posterior is of form PMB. A natural extension of this filter could consider fusion of PMBMs enabling to maintain multiple global hypotheses. In the current filter implementation, measurements from targets which are spatially close to each other are clustered into the same measurement cell with the result that the filter outputs only a single ET. Maintaining multiple global hypotheses together with an efficient data association procedure would mitigate this effect. Furthermore, the fusion step was applied separately on the Poisson RFSs and the MB RFSs for the different types of tracked targets. Future work could consider to directly fuse the PMBMs of each filter. Note that the discussion on target trajectories produced by the filter mentioned in Sec. 6.2 also applies here.

6.4 Author Contributions of Appended Papers

Here, we state the authors contributions of each appended paper.

6.4.1 Paper A

The model was developed in collaboration between M. Fröhle (MF), T. Charalambous (TC) and H. Wymeersch (HW). MF implemented the model and performed the

simulations. HW, TC and I. Nevat (IN) participated in the discussions.

6.4.2 Paper B

MF proposed the model and implemented it. L. S. Muppirisetty (LSM) and HW participated in the discussions.

6.4.3 Paper C

MF and C. Lindberg (CL) proposed and implemented the filter. HW participated in the discussions and collaborated with paper writing.

6.4.4 Paper D

MF and CL proposed the problem. MF derived and implemented the filter, performed the experiment, simulations, and analysis. K. Granström (KG) and HW participated in the discussions.

6.4.5 Paper E

MF implemented the filter and performed the experiments. KG and HW participated in the discussions.

6.4.6 Paper F

MF proposed and implemented the GP model of [30] combined with the ETT filter of [16]. MF proposed and implemented the posterior fusion. HW assisted with the MB fusion for more than two posteriors. KG and HW participated in the discussions.

References

[1] B. J. Julian, M. Angermann, M. Schwager, and D. Rus, "Distributed robotic sensor networks: An information-theoretic approach", *The International Journal of Robotics Research*, vol. 31, no. 10, pp. 1134–1154, 2012.

[2] A. Nayak and I. Stojmenovic, *Wireless sensor and actuator networks: algorithms and protocols for scalable coordination and data communication*. John Wiley & Sons, 2010.

[3] G. Karagiannis, O. Altintas, E. Ekici, G. Heijenk, B. Jarupan, K. Lin, and T. Weil, "Vehicular networking: A survey and tutorial on requirements, architectures, challenges, standards and solutions", *IEEE Communications Surveys Tutorials*, vol. 13, no. 4, pp. 584–616, 2011.

[4] A. A. Zaidi, B. Kulcsár, and H. Wymeersch, "Traffic-adaptive signal control and vehicle routing using a decentralized back-pressure method", in *European Control Conference*, 2015, pp. 3029–3034.

[5] A. Goldsmith, *Wireless communications*. Cambridge university press, 2005.

[6] J. Karedal, N. Czink, A. Paier, F. Tufvesson, and A. F. Molisch, "Path loss modeling for vehicle-to-vehicle communications", *IEEE Transactions on Vehicular Technology*, vol. 60, no. 1, pp. 323–328, 2011.

[7] A. F. Molisch and F. Tufvesson, "Propagation channel models for next-generation wireless communications systems", *IEICE Transactions on Communications*, vol. 97, no. 10, pp. 2022–2034, 2014.

[8] T. S. Rappaport, G. R. MacCartney, M. K. Samimi, and S. Sun, "Wideband millimeter-wave propagation measurements and channel models for future wireless communication system design", *IEEE Transactions on Communications*, vol. 63, no. 9, pp. 3029–3056, 2015.

[9] T. Abbas, K. Sjöberg, J. Karedal, and F. Tufvesson, "A measurement based shadow fading model for vehicle-to-vehicle network simulations", *International Journal of Antennas and Propagation*, vol. 2015, 2015.

[10] O. Renaudin, V.-M. Kolmonen, P. Vainikainen, and C. Oestges, "Wideband measurement-based modeling of inter-vehicle channels in the 5-GHz band.", *IEEE Transations on Vehicular Technology*, vol. 62, no. 8, pp. 3531–3540, 2013.

[11] D. Simon, *Optimal state estimation: Kalman, H infinity, and nonlinear approaches*. John Wiley & Sons, 2006.

[12] Y. Bar-Shalom and X.-R. Li, *Multitarget-multisensor tracking: principles and techniques*. YBs London, UK, 1995, vol. 19.

[13] C. Qiu, Z. Zhang, H. Lu, and H. Luo, "A survey of motion-based multitarget tracking methods", *Progress In Electromagnetics Research*, vol. 62, pp. 195–223, 2015.

[14] K. Granström, M. Baum, and S. Reuter, "Extended object tracking: Introduction, overview, and applications", *JAIF Journal of Advances in Information Fusion*, vol. 12, no. 2, pp. 139–174, 2017.

[15] I. Skog and P. Händel, "In-car positioning and navigation technologies - a survey", *IEEE Transactions on Intelligent Transportation Systems*, vol. 10, no. 1, pp. 4–21, 2009.

[16] K. Granström, M. Fatemi, and L. Svensson, "Poisson multi-Bernoulli conjugate prior for multiple extended object estimation", *arXiv preprint arXiv:1605.06311*, 2016.

[17] ——, "Gamma Gaussian inverse-Wishart Poisson multi-Bernoulli filter for extended target tracking", in *19th International Conference on Information Fusion (FUSION)*, 2016, pp. 893–900.

[18] A. Böttcher, P. Vary, C. Schneider, and R. S. Thomä, "De-correlation distance of the large scale parameters in an urban macro cell scenario", in *6th European Conference on Antennas and Propagation (EUCAP)*, 2012, pp. 1417–1421.

[19] N. Jaldén, "Analysis and Modelling of Joint Channel Properties from Multi-site, Multi-Antenna Radio Measurements", PhD thesis, KTH, Signal Processing, 2010.

[20] G. L. Stüber, *Principles of Mobile Communication*. Springer Science & Business Media, 2011.

[21] M. Neiman, "The principle of reciprocity in antenna theory", *Proceedings of the IRE*, vol. 31, no. 12, pp. 666–671, 1943.

[22] M. Gudmundson, "Correlation model for shadow fading in mobile radio systems", *Electronics Letters*, vol. 27, no. 23, pp. 2145–2146, 1991.

[23] Z. Wang, E. K. Tameh, and A. R. Nix, "Joint Shadowing Process in Urban Peer-to-Peer Radio Channels", *IEEE Transactions on Vehicular Technology*, vol. 57, no. 1, pp. 52–64, 2008.

[24] Z. Li, R. Wang, and A. F. Molisch, "Shadowing in Urban Environments with Microcellular or Peer-to-Peer Links", in *6th European Conference on Antennas and Propagation (EUCAP)*, 2012, pp. 44–48.

[25] C. M. Bishop, *Pattern Recognition and Machine Learning*. Springer, 2006.

[26] C. E. Rasmussen and C. K. I. Williams, *Gaussian processes for machine learning*. MIT Press, 2006.

[27] P. Dallaire, C. Besse, and B. Chaib-draa, "An approximate inference with Gaussian process to latent functions from uncertain data", *Neurocomputing*, vol. 74, no. 11, pp. 1945–1955, 2011.

[28] A. Girard, "Approximate methods for propagation of uncertainty with Gaussian process models", PhD thesis, University of Glasgow, 2004.

[29] L. S. Muppirisetty, T. Svensson, and H. Wymeersch, "Spatial wireless channel prediction under location uncertainty", *IEEE Transactions on Wireless Communications*, vol. 15, no. 2, pp. 1031–1044, 2016.

[30] N. Wahlström and E. Özkan, "Extended target tracking using Gaussian processes", *IEEE Transactions on Signal Processing*, vol. 63, no. 16, pp. 4165–4178, 2015.

[31] M. S. Arulampalam, S. Maskell, N. Gordon, and T. Clapp, "A tutorial on particle filters for online nonlinear/non-Gaussian Bayesian tracking", *IEEE Transactions on Signal Processing*, vol. 50, no. 2, pp. 174–188, 2002.

[32] S. M. Kay, *Fundamentals of statistical signal processing, volume I: estimation theory*. Prentice Hall, 1993.

[33] A. Doucet and A. M. Johansen, "A tutorial on particle filtering and smoothing: Fifteen years later", *Handbook of nonlinear filtering*, vol. 12, no. 656-704, p. 3, 2009.

[34] S. Haykin, *Cognitive dynamic systems: perception-action cycle, radar and radio*. Cambridge University Press, 2012.

[35] S. J. Julier and J. K. Uhlmann, "New extension of the Kalman filter to nonlinear systems", in *Signal processing, sensor fusion, and target recognition VI*, International Society for Optics and Photonics, vol. 3068, 1997, pp. 182–194.

[36] ——, "Unscented filtering and nonlinear estimation", *Proceedings of the IEEE*, vol. 92, no. 3, pp. 401–422, 2004.

[37] Y. Bar-Shalom, P. K. Willett, and X. Tian, *Tracking and data fusion: A handbook of algorithms*. Storrs, CT: YBS Publishing, 2011.

[38] R. Mahler and A. El-Fallah, "Bayesian unified registration and tracking", in *Signal Processing, Sensor Fusion, and Target Recognition XX*, International Society for Optics and Photonics, vol. 8050, 2011, 80500H.

[39] F. Meyer, O. Hlinka, H. Wymeersch, E. Riegler, and F. Hlawatsch, "Distributed localization and tracking of mobile networks including noncooperative objects", *IEEE Transactions on Signal and Information Processing over Networks*, vol. 2, no. 1, pp. 57–71, 2016.

[40] H. Durrant-Whyte and T. Bailey, "Simultaneous localization and mapping: Part i", *IEEE robotics & automation magazine*, vol. 13, no. 2, pp. 99–110, 2006.

[41] S. Särkkä, *Bayesian filtering and smoothing*. Cambridge University Press, 2013, vol. 3.

[42] A. Doucet, N. De Freitas, K. Murphy, and S. Russell, "Rao-Blackwellised particle filtering for dynamic Bayesian networks", in *Proceedings of the Sixteenth conference on Uncertainty in artificial intelligence*, Morgan Kaufmann Publishers Inc., 2000, pp. 176–183.

[43] K. P. Murphy, "Bayesian map learning in dynamic environments", in *Advances in Neural Information Processing Systems*, 2000, pp. 1015–1021.

[44] C. Cadena, L. Carlone, H. Carrillo, Y. Latif, D. Scaramuzza, J. Neira, I. Reid, and J. J. Leonard, "Past, present, and future of simultaneous localization and mapping: Toward the robust-perception age", *IEEE Transactions on Robotics*, vol. 32, no. 6, pp. 1309–1332, 2016.

[45] H. Wymeersch, *Iterative receiver design*. Cambridge Univ. Press, 2007.

[46] J. Williams and R. Lau, "Approximate evaluation of marginal association probabilities with belief propagation", *IEEE Transactions on Aerospace and Electronic Systems*, vol. 50, no. 4, pp. 2942–2959, 2014.

[47] J. L. Williams and R. A. Lau, "Convergence of loopy belief propagation for data association", in *Proceedings of the IEEE 6th International Conference on Intelligent Sensors, Sensor Networks and Information Processing*, 2010, pp. 175–180.

[48] F. Meyer, P. Braca, P. Willett, and F. Hlawatsch, "A scalable algorithm for tracking an unknown number of targets using multiple sensors", *IEEE Transactions on Signal Processing*, vol. 65, no. 13, pp. 3478–3493, 2017.

[49] C.-Y. Chong, S. Mori, W. H. Barker, and K.-C. Chang, "Architectures and algorithms for track association and fusion", *IEEE Aerospace and Electronic Systems Magazine*, vol. 15, no. 1, pp. 5–13, 2000.

[50] J. K. Uhlmann, "General data fusion for estimates with unknown cross covariances", in *Signal Processing, Sensor Fusion, and Target Recognition V*, International Society for Optics and Photonics, vol. 2755, 1996, pp. 536–548.

[51] S. J. Julier and J. K. Uhlmann, "A non-divergent estimation algorithm in the presence of unknown correlations", in *American Control Conference, 1997. Proceedings of the 1997*, IEEE, vol. 4, 1997, pp. 2369–2373.

[52] R. P. Mahler, "Optimal/robust distributed data fusion: A unified approach", in *Signal Processing, Sensor Fusion, and Target Recognition IX*, International Society for Optics and Photonics, vol. 4052, 2000, pp. 128–139.

[53] F. Meyer, T. Kropfreiter, J. L. Williams, R. Lau, F. Hlawatsch, P. Braca, and M. Z. Win, "Message passing algorithms for scalable multitarget tracking", *Proceedings of the IEEE*, vol. 106, no. 2, pp. 221–259, 2018.

[54] R. L. Streit and T. E. Luginbuhl, "Probabilistic multi-hypothesis tracking", Naval Underwater Systems Center Newport RI, Tech. Rep., 1995.

[55] M. Fröhle, C. Lindberg, and H. Wymeersch, "Cooperative localization of vehicles without inter-vehicle measurements", in *IEEE Wireless Communications and Networking Conference (WCNC)*, IEEE, 2018, pp. 1–6.

[56] F. Meyer, P. Braca, P. Willett, and F. Hlawatsch, "Scalable multitarget tracking using multiple sensors: A belief propagation approach", in *Proceedings ot the 18th International Conference on Information Fusion*, 2015, pp. 1778–1785.

[57] R. P. Mahler, *Statistical multisource-multitarget information fusion*. Artech House, Inc., 2007.

[58] J. L. Williams, "Marginal multi-Bernoulli filters: RFS derivation of MHT, JIPDA, and association-based MeMBer", *IEEE Transactions on Aerospace and Electronic Systems*, vol. 51, no. 3, pp. 1664–1687, 2015.

[59] R. P. Mahler, *Advances in Statistical Multisource-Multitarget Information Fusion*. Artech House, Inc., 2014.

[60] Á. F. García-Fernández, J. L. Williams, K. Granström, and L. Svensson, "Poisson multi-Bernoulli mixture filter: direct derivation and implementation", *IEEE Transactions on Aerospace and Electronic Systems*, pp. 1–1, 2018.

[61] B.-N. Vo and W.-K. Ma, "The Gaussian mixture probability hypothesis density filter", *IEEE Transactions on Signal Processing*, vol. 54, no. 11, pp. 4091–4104, 2006.

[62] B.-N. Vo, S. Singh, and A. Doucet, "Sequential Monte Carlo methods for multitarget filtering with random finite sets", *IEEE Transactions on Aerospace and electronic systems*, vol. 41, no. 4, pp. 1224–1245, 2005.

[63] B. T. Vo, B.-N. Vo, and A. Cantoni, "The cardinality balanced multi-target multi-Bernoulli filter and its implementations", *IEEE Transactions on Signal Processing*, vol. 57, no. 2, pp. 409–423, 2009.

[64] B.-T. Vo and B.-N. Vo, "Labeled random finite sets and multi-object conjugate priors", *IEEE Transactions on Signal Processing*, vol. 61, no. 13, pp. 3460–3475, 2013.

[65] S. Reuter, B.-T. Vo, B.-N. Vo, and K. Dietmayer, "The labeled multi-Bernoulli filter", *IEEE Transactions on Signal Processing*, vol. 62, no. 12, pp. 3246–3260, 2014.

[66] K. Granström, L. Svensson, Y. Xia, J. Williams, and Á. F. García-Femández, "Poisson multi-Bernoulli mixture trackers: Continuity through random finite sets of trajectories", in *21st International Conference on Information Fusion (FUSION)*, IEEE, 2018, pp. 1–5.

[67] Y. Xia, K. Granström, L. Svensson, and Á. F. García-Fernández, "An implementation of the Poisson multi-Bernoulli mixture trajectory filter via dual decomposition", in *21st International Conference on Information Fusion (FUSION)*, IEEE, 2018, pp. 1–8.

[68] L. Svensson and M. Morelande, "Target tracking based on estimation of sets of trajectories", in *17th International Conference on Information Fusion (FUSION)*, IEEE, 2014, pp. 1–8.

[69] Á. F. García-Fernández, L. Svensson, and M. R. Morelande, "Multiple target tracking based on sets of trajectories", *arXiv preprint arXiv:1605.08163*, 2016.

[70] Á. F. García-Fernández and L. Svensson, "Trajectory probability hypothesis density filter", in *21st International Conference on Information Fusion (FUSION)*, IEEE, 2018, pp. 1430–1437.

[71] Á. F. García-Fernández, J. L. Williams, K. Granström, and L. Svensson, "Poisson multi-bernoulli mixture filter: Direct derivation and implementation", *IEEE Transactions on Aerospace and Electronic Systems*, 2018.

[72] Y. Xia, K. Granström, L. Svensson, and Á. F. García-Fernández, "Performance evaluation of multi-Bernoulli conjugate priors for multi-target filtering", in *20th International Conference on Information Fusion (Fusion)*, IEEE, 2017, pp. 1–8.

[73] J. L. Williams, "An efficient, variational approximation of the best fitting multi-Bernoulli filter", *IEEE Transactions on Signal Processing*, vol. 63, no. 1, pp. 258–273, 2015.

[74] T. Kropfreiter, F. Meyer, and F. Hlawatsch, "Sequential Monte Carlo implementation of the track-oriented marginal multi-Bernoulli/Poisson filter", in *19th International Conference on Information Fusion (FUSION)*, IEEE, 2016, pp. 972–979.

[75] B. Ristic, D. E. Clark, and N. Gordon, "Calibration of multi-target tracking algorithms using non-cooperative targets", *IEEE Journal of Selected Topics in Signal Processing*, vol. 7, no. 3, pp. 390–398, 2013.

[76] S. J. Julier and A. Gning, "Bernoulli filtering on a moving platform", in *18th International Conference on Information Fusion (Fusion)*, IEEE, 2015, pp. 1511–1518.

[77] J. Mullane, B.-N. Vo, M. D. Adams, and B.-T. Vo, "A random-finite-set approach to Bayesian SLAM", *IEEE Transactions on Robotics*, vol. 27, no. 2, pp. 268–282, 2011.

[78] E. Brekke, B. Kalyan, and M. Chitre, "A novel formulation of the Bayes recursion for single-cluster filtering", in *2014 IEEE Aerospace Conference*, IEEE, 2014, pp. 1–16.

[79] H. Deusch, S. Reuter, and K. Dietmayer, "The labeled multi-Bernoulli SLAM filter", *IEEE Signal Processing Letters*, vol. 22, no. 10, pp. 1561–1565, 2015.

[80] J. A. Castellanos, J. D. Tardós, and G. Schmidt, "Building a global map of the environment of a mobile robot: The importance of correlations", in *1997 IEEE International Conference on Robotics and Automation*, IEEE, vol. 2, 1997, pp. 1053–1059.

[81] K. Granström and U. Orguner, "Estimation and maintenance of measurement rates for multiple extended target tracking", in *15th International Conference on Information Fusion (FUSION)*, IEEE, 2012, pp. 2170–2176.

[82] L. Hammarstrand, L. Svensson, F. Sandblom, and J. Sorstedt, "Extended object tracking using a radar resolution model", *IEEE Transactions on Aerospace and Electronic Systems*, vol. 48, no. 3, pp. 2371–2386, 2012.

[83] L. Hammarstrand, M. Lundgren, and L. Svensson, "Adaptive radar sensor model for tracking structured extended objects", *IEEE Transactions on Aerospace and Electronic Systems*, vol. 48, no. 3, pp. 1975–1995, 2012.

[84] J. W. Koch, "Bayesian approach to extended object and cluster tracking using random matrices", *IEEE Transactions on Aerospace and Electronic Systems*, vol. 44, no. 3, 2008.

[85] M. F. Huber, "Recursive Gaussian process: On-line regression and learning", *Pattern Recognition Letters*, vol. 45, pp. 85–91, 2014.

[86] W. Aftab, A. De Freitas, M. Arvaneh, and L. Mihaylova, "A Gaussian process approach for extended object tracking with random shapes and for dealing with intractable likelihoods", in *22nd International Conference on Digital Signal Processing (DSP)*, IEEE, 2017, pp. 1–5.

[87] E. Özkan, N. Wahlström, and S. J. Godsill, "Rao-Blackwellised particle filter for star-convex extended target tracking models", in *19th International Conference on Information Fusion (FUSION)*, IEEE, 2016, pp. 1193–1199.

[88] T. Hirscher, A. Scheel, S. Reuter, and K. Dietmayer, "Multiple extended object tracking using Gaussian processes", in *19th International Conference on Information Fusion (FUSION)*, IEEE, 2016, pp. 868–875.

[89] G. Battistelli, L. Chisci, C. Fantacci, A. Farina, and A. Graziano, "Consensus CPHD filter for distributed multitarget tracking", *IEEE Journal of Selected Topics in Signal Processing*, vol. 7, no. 3, pp. 508–520, 2013.

[90] D. Clark, S. Julier, R. Mahler, and B. Ristic, "Robust multi-object sensor fusion with unknown correlations", in *Sensor Signal Processing for Defence (SSPD)*, 2010.

[91] B. Wang, W. Yi, R. Hoseinnezhad, S. Li, L. Kong, and X. Yang, "Distributed fusion with multi-Bernoulli filter based on generalized covariance intersection", *IEEE Transactions on Signal Processing*, vol. 65, no. 1, pp. 242–255, 2017.

[92] H. Bijl, T. B. Schön, J.-W. van Wingerden, and M. Verhaegen, "System identification through online sparse Gaussian process regression with input noise", *IFAC Journal of Systems and Control*, vol. 2, pp. 1–11, 2017.

[93] C. E. Rasmussen, "Gaussian processes in machine learning", in *Advanced lectures on machine learning*, 2004, pp. 63–71.